Prediction of Radioactive Injection Dosage for PET Image

By
Ebtesam Ahmad Saeed Alsanea

A thesis submitted for the requirements of the degree of Master of Computer Science

Supervised By
Dr. Wadee Saleh Alhalabi

FACULTY OF COMPUTING AND INFORMATION TECHNOLOGY
KING ABDULAZIZ UNIVERSITY
JEDDAH – SAUDI ARABIA
Shabaan1437H – MAY 2016G

بسم الله الرحمن الرحيم

﴿الْحَمْدُ لِلَّهِ الَّذِي هَدَانَا لِهَذَا وَمَا كُنَّا لِنَهْتَدِيَ لَوْلَا أَنْ هَدَانَا اللَّهُ ﴾

سورة الأعراف(٤٣)

Prediction of Radioactive Injection Dosage for PET Image

By
Ebtesam Ahmad Saeed Alsanea

A thesis submitted for the requirements of the degree of Master of Computer Science

Supervised By
Dr. Wadee Saleh Alhalabi

FACULTY OF COMPUTING AND INFORMATION TECHNOLOGY
KING ABDULAZIZ UNIVERSITY
JEDDAH – SAUDI ARABIA
Shabaan 1437H – May 2016G

التنبؤ بجرعة المادة المشعة المناسبة للحقن في التصوير المقطعي النيتروني

ابتسام أحمد سعيد الصانع

بحث مقدم لنيل درجة الماجستير في علوم الحاسبات

إشراف:
د. وديع صالح الحلبي

كلية الحاسبات و تقنية المعلومات
جامعة الملك عبد العزيز
جدة – المملكة العربية السعودية
شعبان ١٤٣٧هـ - مايو ٢٠١٦م

Prediction of Radioactive Injection Dosage for PET Image

By
Ebtesam Ahmad Saeed Alsanea

A thesis submitted for the requirements of the degree of Master of Computer Science

EXAMINATION COMETEE

	Name	Rank	Field	Signature
Internal Examiner	Dr. Fadi Fouad Foz	Professor	Computer Science	
External Examiner	Dr. Ali Hussein Morfeq	Associate Professor	Electrical Engineering and Computer Engineering	
Advisor	Dr. Wadee Saleh Alhalabi	Associate Professor	Computer Science	

KING ABDULAZIZ UNIVERSITY
Shabaan 1437H – May 2016 G

التنبؤ بجرعة المادة المشعة المناسبة للحقن في التصوير المقطعي النيتروني

ابتسام أحمد سعيد الصانع

بحث مقدم لنيل درجة الماجستير في علوم الحاسبات

لجنة المناقشة و الحكم على الرسالة

	الاسم	المرتبة العلمية	التخصص	التوقيع
عضو داخلي	**د .فادي فؤاد فوز**	**أستاذ**	**علوم حاسبات**	
عضو خارجي	**د .علي حسين مرفق**	**أستاذ مشارك**	**الهندسة الكهربائية وهندسة الحاسبات**	
مشرف رئيس	**د .وديع صالح الحلبي**	**أستاذ مشارك**	**علوم حاسبات**	

جامعة الملك عبد العزيز
شعبان ١٤٣٧هـ - مايو ٢٠١٦م

Dedicated to

The memory of my parents ..
I am grateful for the live you gave me..
You helped me to become the person I am today..
I LOVE & MISS YOU

ACKNOWLEDGMENTS

In the Name of Allah, the Most Merciful, the Most Compassionate, all praise be to Allah, the Lord of the Worlds, and prayers and peace be upon Mohamed, His servant and messenger.

Above all, I would like to thanks ALLAH , who is the source of everything .

Then I would like to thanks all people who have supported me from the beginning to the compilation of this long journey

First of all , my acknowledgements and many thanks go to my supervisor **Dr.Wadee Alhalabi** for his patient , kindness , availability and guiding.

Secondly, many thanks to my brothers (**Majed and Saeed**) for always believing in me and supporting me.

My special thanks goes to the warmest brother ever, **Mohammed.**

My big big thanks goes to my sisters for being always lovely and patient. For lessening to my never ending education problems and showing interest.

Thanks to my mother warm hearts ...**Aisha and Maha**

Thanks to my litter sister , my friend , my twin, **Bushra**

Last but not least ,My family : without your support , I would never been where I am now,

Thank you all for having always effort to give me the best

Prediction of Radioactive Injection Dosage for PET Image

Ebtesam Ahmad Saeed Alsanea

Abstract

Advanced computer and imaging techniques find extensive use in medicine. Medical imaging modalities such as Positron Emission Tomography (PET) are becoming an increasingly important component of clinical applications and research oncology for diagnosis, treatment planning, and tumor monitoring to gather details about the process of the patient body whether it is a disease or normal physiological process.

An important aspect of PET imaging in clinical application is the localization and detection of tumors and lesions by administering a predetermined amount of radiotracer. This procedure allows, for example, a detailed view of what is going inside the patient body in cellular level. The quality of PET image is strongly dependent on the amount of administrated radiotracer and the patient's body parameters. As the amount of injection radiotracer increases, the quality of resulting image increases and the lesion detection efficiency increases.

The PET examiner society recognizes that any dose of radiotracer is associated with some possible radiation risks. It can be harmful to the patient if essential PET imaging session is not made due to fear of radiation risk. In order to ensure the highest quality diagnosis and the smallest radiation risk, the patient should receive the smallest amount of radiotracer that provides an image with sufficient quality.

Our study is focused on proposing an efficient PET simulation tool that predicts the smallest possible amount of administrated radiotracer to provides the appropriate diagnostic information based on significant patient's body parameters (weight, age) at fixed scanning to improve the clinical diagnostic process in term of tumor-detecting and localization.

We have built a model of particular PET scanner and model of a patient based on real MRI image and digital anthropomorphic phantom of our region of interest (brain). We have performed Monte Carlo simulation for whole PET procedure with a special parameter. At Ivalidation stage, we have analyzed the system performance (in term of spatial resolution, sensitivity, and scatter fraction). In evaluating stage, a dataset of 60 patients is used, and 11 independent dose prediction simulations for each patient are performed.

We conclude that our simulator performs a desirable and efficient prediction of injection radiotracer amount that optimizes the current clinical amount up to 28%. In addition, we found that the total injected radiotracer dosage for adult patients are mostly affected when considering patient weight rather than patient age.

.

TABLE OF CONTENTS

DEDICATION i
ACKNOWLEDGMENTS ii
ABSTRACT iii
TABLE OF CONTENTS iv
LIST OF FIGURES vi
LIST OF TABLES viii
LIST OF SYMBOLS AND TERMINOLOGY ix
CHAPTER 1 : INTRODUCION 1

1.1 Introduction 2
1.2 Problem Statement 5
1.3 Thesis objectives 5
1.4 Thesis Organization 6

CHAPTER 2 :LITERATURE REVIEW 7

2.1 Background 8
2.2 Principles of Nuclear Medicine Imaging 8
2.3 Positron Emission Tomography PET 9

2.3.1 Photon Interaction with Patient's Body 11
2.3.2 PET Detectors 12
2.3.3 PET Acquisition Protocols 14
2.3.4 PET Data Representation 15
2.3.5 PET Image Reconstruction 16

2.3.5.1 Analytical Reconstruction 17
2.3.5.2 Iterative Reconstruction 20

2.3.6 PET Radiotracers 21

2.3.6.1 Radiotracer Injection Dose 23

2.4 Phantom 24
2.5 Monte Carlo Method in Emission Tomography 25

2.5.1 Monte Carlo Simulations Software 29

CHAPTER 3 :METHODOLGY 31

3.1 Introduction 32
3.2 Patient Model 33

3.2.1 The Phantom 34
3.2.2 Phantom Builds from Real Data 34
3.2.3 Radiotracer Injection Dose Calculation 35

3.2.4 Phantom Simulation Process 36
3.2.4.1 Adding Tumors and Lesions 39
3.3 Scanner Model 39
3.4 PET Process Simulation 40
3.4.1 Positron Emission and Annihilation 40
3.4.1.1 Positron Emission Direction 42
3.4.1.2 Positron Annihilation Point Coordination 42
3.4.2 Photon transportation 43
3.4.3 Photon Detection 44
3.4.4 Sinogram Formation 44
3.4.4.1 Sinogram Building Process 46
3.5 PET Image Reconstruction 47
3.5.1.1 Fusion of the PET Reconstructed Image 48
3.6 Image Quality Assessment 49
3.6.1 Signal to Noise Ratio 49
3.6.2 Noise Equivalent Count 49
3.6.3 Performance Measurement 50
CHAPTER 4 :RESULTS 52
4.1 Introduction 53
4.2 Technical Requirements 53
4.3 Experiments and Results 54
4.3.1 Patient Model 54
4.3.2 Scanner Model 59
4.3.3 Simulated PET Image Quality Assessment 63
CHAPTER 5 :DISCUSSIONS 70
5.1 Introduction 71
5.2 Patient Model 71
5.3 Scanner Model 72
5.4 Simulated PET Image Quality Assessment 74
5.5 Execution Time 79
CHAPTER 6 :CONCLUSION & FUTURE WORK 80
6.1 Conclusion 81
6.2 Limitation 82
6.3 Future Work 82
LIST OF REFERENCES 84
المستخلص 91

LIST OF FIGURES

CHAPTER 2: LITERATURE REVIEW

Figure 2.1 PET imaging procedure details..... 11
Figure 2.2 Coincidences events..... 11
Figure 2.3 PET detectors configuration..... 13
Figure 2.4 PET scanner configuration..... 13
Figure 2.5 The coordinates of the Lines of Response in a Sinogram..... 15
Figure 2.6 A parallel projection, for a specific angle ϕ , of an object corresponds to a row s in the sinogram matrix..... 16
Figure 2.7 Basic step of reconstructed image filtering..... 19
Figure 2.8 Iterative reconstruction technique..... 21
Figure 2.9 FDG radiotracer metabolism in cells..... 23
Figure 2.10 Voxlized phantom..... 25
Figure 2.11 Monte Carlo simulation applied to PET imaging system..... 29

CHAPTER 3: METHODOLOGY

Figure 3.1 PET simulation basic structure..... 32
Figure 3.2 Digital voxlized phantom..... 34
Figure 3.3 Radiotracer injection dose calculation process..... 36
Figure 3.4 SimSET activity distribution table for 18F-FDG radiotracer activity in Zubal phantom..... 38
Figure 3.5 PET physical processes implementing in the simulation..... 40
Figure 3.6 positron range for 18F-FDG in water..... 41
Figure 3.7 Sinogram building process..... 45
Figure 3.8 Reconstruction of single detector crystal..... 48
Figure 3.9 Confusion matrix..... 51

CHAPTER 4: RESULTS

Figure 4.1 MRI brain image from DICOM library..... 55
Figure 4.2 Metadata associated with MRI image presented in Figure 4.1..... 56
Figure 4.3 Original MRI phantom image for the proposed patient model..... 58
Figure 4.4 MRI phantom for the proposed Patient model after excluding non-cerebral structures..... 58
Figure 4.5 Attenuation coefficient map for the proposed patient model..... 58
Figure 4.6 Emission map of the proposed patient model when the total injected radiotracer amount = 370MBq..... 59
Figure 4.7 Emission map of the proposed patient model when the total injected radiotracer amount = 600MBq..... 59
Figure 4.8 Physical and simulated illustration of the proposed scanner model..... 60

Figure 4.9 Direction at which spatial resolution measured..... 61
Figure 4.10 True and detected tumours when recall=1..... 67
Figure 4.11 True and detected tumor when recall=1 (detailed view)..... 67
Figure 4.12 Image-based lesion detection experiments of 11 independent simulations for patient with 63Kg and 70 years..... 68

CHAPTER 5: DISCUSSIONS

Figure 5.1 Spatial resolution for phantom positioned at 10 mm from the center of scanner ring..... 73
Figure 5.2 Spatial resolution for phantom positioned at 100 mm from the center of scanner ring..... 73
Figure 5.3 Sensitivity values for phantoms positioned at 0 and 100 mm from the center of scanner ring..... 74
Figure 5.4 Scatter fraction evaluation measurement for two energy windows..... 74
Figure 5.5 NEC values for default scanner and patient model..... 75
Figure 5.6 Lesion detection (precision and recall) for default patient model..... 76
Figure 5.7 Total injected activity for patients with different weight (Kg) and fixed age (=35 years)..... 76
Figure 5.8 Total injected activity for different patients groups..... 77
Figure 5.9 Total injected activity for patients with fixed weight (Kg) and different age (years) weight=63 Kg..... 78
Figure 5.10 PET simulation execution time profile..... 79

LIST OF TABLES

Table 2.1 Selected list of isotopes, and their decay energy by positron emission..... 9

Table 2.2 Some radiotracers used in PET imaging and their applications..... 22

Table 3.1 Example of attenuation coefficient of the structures in Zubal phantom..... 37

Table 3.2 Index numbers and their associated structures in Phantom under study.....38

Table 3.3 Detectors ring arrangement..... 46

Table 4.1 Specifications and features of the Siemens Biograph2 scanning system....60

Table 4.2 Spatial resolution for two different phantom positioned at 10 and 100 mm from the center of the proposed scanner model.....61

Table 4.3 Simulated and measured values of the sensitivity of our proposed scanner model..... 62

Table 4.4 Simulated and measured value of the scatter fraction experiment of our proposed scanner model..... 63

Table 4.5 Statistical parameters SNR and NEC for default scanner and patient model..... 64

Table 4.6 Lesion detection (precision and recall) for default patient model..... 65

Table 4.7 total injected activity for patients with different weight in Kg and fixed age in year, age=35 years.....66

Table 4.8 Total injected activity for patients with fixed weight in Kg and different age in year, weight=63 Kg.....66

Table 4.9 Precision and recall values image-based lesion detection experiments of 11 independent simulations for patient with 63Kg and 70 years.....69

LIST OF SYMBOLS AND TERMINOLOGY

ALARA	As Low As Reasonable Achievable
BP	Back Projection
Bq	Becquerel
CDF	Cumulative Distribution Function
Ci	Curie
CT	Computed Tomography
DICOM	Digital Imaging and Communication in Medicine
EANM	European Association of Nuclear Medicine
FBP	Filter Back Projection
FDG	Fluro-Deoxy-Glucose
GATE	Geeant4 Application for Emission Tomography
IA	Injected Activity
LOR	Line Of Response
MRI	Magnetic Resonance imaging
NEC	Noise Equivalent Count
NEMA	National Electronic Manufacture Association
OSEM	Order Subset Expectation Maximization Algorithm
PD	Probability Distribution
PET	Positron Emission Tomography
PR	Positron Range
RNG	Random Number Generator
SI	International System of unit
SimSET	Simulation System for Emission Tomography
SNR	Signal to Noise Ratio
SPECT	Single Photon Emission Computed Tomography
UD	Uniform Distribution

1 INTRODUCION

CHAPTER I

INTRODUCTION

1.1 Introduction

Medical imaging is becoming an increasingly important component of clinical applications and research oncology for diagnosis treatment planning, and tumor monitoring. During the years, multiple imaging technologies have been developed using the rapid advances in computer and imaging approaches. The non-invasive clinical diagnose can be perform with two types of different medical imaging technologies: standard and functional. Technologies such as X-ray radiography, Computed Tomography (CT) , Ultra Sound (US) and Magnetic Resonance imaging (MRI) provide anatomical information about morphological changes of size, shape or location in a patient's body. On the other hand, technologies such as functional MRI, Single Photon Emission Computed Tomography (SPECT), Positron Emission Tomography (PET) and gamma PET provide functional information about biological function of the body. Recently, powerful imaging technique that combine the two technologies (for example PET/MRI) were developed in order to achieve a more accurate fusion image and a complete picture that can be used to diagnose problems and determine the treatment progress[1], [2].

Nuclear medicine examinations are invasive and repeatable reproducible imaging methods widely applied in the field of cardiology, oncology and neuroscience. These methods integrate two main components in order to work properly: radiotracer and detector. The radiotracer administered to the patient's body has a marked radionuclide emitting a positron in PET and a single photon in SPECT. The second component is represented by a camera able to detect the emitted radionuclide. In PET, the ^{18}F, ^{11}C, ^{13}N and ^{15}O are the positron emitting radionuclide that are usually used in medicine application. These radiotracers are attracted to specific organs, tissues or body regions and enable the measurement of the biological and biochemical process. The camera detects the radiotracer presence and generates images by detecting the photons annihilated from positron emission and decay. The generated pictures are highly sensitive and quantitatively accurate images of the tracer concentration distribution, which allow doctors and specialists to follow the dynamics of the tracer in the patient's body / region of interest. The most common radiotracer used in PET examination is 2-Deoxy-[^{18}F]Floro-D-Glucose ([^{18}F]FDG, ^{18}F-FDG or FDG). As FDG is analogous to glucose and tumours accumulate glucose more than the surrounded healthy tissues, it is used to stage cancer and to detect possible tumors. The PET functional imaging using FDG is considered as the most common application in medical practice for examination and diagnosis of oncologic patients[3]–[5].

Because PET imaging deals with radiotracer decay, positron emission, photon transportation and particles detection, the use of simulation is very popular in PET research and clinical practice. Monte Carlo simulation technique plays an essential role in nuclear medicine researches and studies covering a wide range of problems that could not solved with experimental or analytical method. Monte Carlo

simulations are widely used for PET imaging simulation because they take into consideration all the random processes concerning in PET imaging. PET simulation tools using Monte Carlo are useful in modelling new scanners, quantifying the radiotracer amount, planning the radiotracer dosage, as well as studying the factors that affect the quality of PET reconstructed image. Furthermore, the Monte Carlo simulation can create data very close to those obtained from real measurement. Currently available Monte Carlo simulation tools are not easy to understand and use by beginners and temporary users with no programming and physical background. Also, those software are extremely time consuming, require large space on the hard disk and in general are consumers of high computational resources[6]–[9].

An important aspect of PET imaging in clinical application is the localization and detection of tumors and lesions by administering a predetermined amount of radiotracer. This allows for example, a detailed view of what is going inside the individual patient's structures and organs at cellular level. The quality of the resulting PET image is strongly dependent on the amount of administrated radiotracer and on other factors such as scanning session duration and the patient's body parameters. As the amount of injection radiotracer increases, the quality of resulting image increases and the lesion detection efficiency increases. The radiotracer dose recommended to be used in real clinical examination is linearly dependent on patient weight and it is not sufficient to produce quality images that can make a difference in diagnosis process[10]–[14].

There are many PET image quality measurements. The widely used metrics are: i)Noise Equivalent Count (NEC), which quantifies the statistical properties of image before construction; and ii) Signal to Noise Ratio (SNR), which measures the noise in the resulting image. From the medical point of view, the most important quality

measurement metric is performance measurement in a given diagnostic task such as lesion localization and detecting[10], [13], [15].

1.2 Problem Statement

In PET imaging procedure, a small amount of radiotracer should be injected in order to examine the body functional process. The PET examiner society recognizes that any dose of radiotracer used in this procedure is associated with some possible radiation risks. The radiation dose for PET imaging should be minimized so that the patient receives the smallest amount of radiotracer that provides image with sufficient quality.

It can harmful to the patient if essential PET imaging session (PET imaging session that can provide to the medic important data about the patient's treatment and diagnosis) is not made due to fear of radiation risk. To ensure the highest quality diagnosis and the smallest radiation risk, the right PET imaging procedure with the right injection dose should be given to the right patient at the right time. When PET imaging examination is performed correctly, the advantages of this examination are more important than the potential risk. Having a computer based software or simulation tool that can predict the optimal radiotracer injected dosage for patients can reduce PET imaging cost and save patients from potential risks.

1.3 Thesis objectives

This This research proposes straightforward, inexpensive, and efficient PET simulation tool. This tool will be used to predict the smallest possible amount of administrated radiotracer that provides the appropriate diagnostic information based on significant patient's body parameters (weight, age) at fixed scanning time. In

addition, this tool will be used to improve the clinical diagnostic process in term of tumor-detecting and localization.

1.4 Thesis Organization

The thesis is organized into six chapters. Chapter 2 provides a literature review about the main principle of nuclear medicine imaging with Particular attention to PET imaging modality. In addition, Chapter 2 focuses on the basic structure of PET imaging system and its general modules, the PET image reconstruction methods the PET radiotracer and its injection dose. Also, it describes the role of Monte Carlo methods in PET imaging. Chapter 3 discusses the methodology followed in this study in details. In chapter 4, all the experiments and results finding are illustrated. Detailed discussions and analyze the results are in chapter 5. Chapter 6 conclude the work, with special emphasis on results and limitation. In addition, some directions for future work are suggested.

2 LITERATURE REVIEW

CHAPTER II

LITERATURE REVIEW

2.1 Background

Since the late 40s, the first application of nuclear imaging was realized when iodine radioactive was used to trace thyroid cancer in a point-by-point scanner. From that point on, due to rapid advances in computing and imaging technologies, different modalities have been developed in nuclear imaging device and applications. PET and SPECT are the main nuclear medicine imaging applications designed to observe the metabolic processes of the body.

In this chapter, a brief overview of the main working principles of nuclear medicine imaging is presented. Particular attention is given to PET imaging and its applications.

2.2 Principles of Nuclear Medicine Imaging

In order to properly work, all nuclear imaging approaches require two key components: i) *a radiopharmaceutical (radiotracer)* that is a label substance made up of a molecule of interest from the patient's body. It is usually introduced into the body by injection, swallowing or even by annihilation then attracted to specific tissues, organs, or body region of interest. ii) *a device or camera (scanner*)able to detect the radiotracer activity presence and that provides functional information

about the processes taking place in that specific region of interest. The information provided by nuclear medicine imaging differs from other medical imaging modalities such as X-ray, CT, and MRI. While these modalities provide an anatomical information about the structure morphological changes, the nuclear medicine imaging provides information about biological activities and biochemical changes of the process[11], [16], [17]. Because the biological activities and biochemical changes exceed the morphological changes, medicine nuclear imaging determines the presence of abnormality much earlier than other approaches [1], [2].

2.3 Positron Emission Tomography PET

PET is described as one of the main applications of nuclear medicine imaging. It is a medical imaging approach that estimates the spatial distribution of the injected radiotracer based on the annihilation of the photons emitted by positron emitting isotopes e.g. ^{11}C, ^{13}N, ^{15}O, ^{18}F, ^{64}Cu. Because the amount of radiotracer introduced to the patient's body is relatively small, PET provides a biochemical and functional diagnose information in non-invasive and safety manner.

The procedure of how PET imaging works is describing as following: the radioactive isotope contained in the injected radiotracer decay through the most common decay method known as positron emission (also called β^+ or beta-plus decay). Essentially, the proton in the isotope converts into a positron e^+ and neutron *n*. Equation (2.1) illustrate an example of isotope's decay by positron emission[5].

$$A_z \rightarrow A_{z-1} + n + e^+ + energy \tag{2.1}$$

The energy is shared between the resulting isotope, the positron, and the neutron. The range of this energy is from zero to maximum value E_{max}. The E_{max} value determined by the difference in atomic masses between the decayed isotope and the resulting one [18]. Table 2.1 presents a list of isotopes that commonly decay by

positron emission method in PET imaging and their associated maximum energy of the emitted positron.

Table 2. 1 Selected list of isotopes, and their decay energy by positron emission

Isotop	Maximum Energy E_{max}
^{11}C	0.96
^{13}N	1.20
^{15}O	1.73
^{18}F	0.63
^{22}Na	0.55
^{64}Cu	0.65

After a short period of time (approximately 10^{-9} s), this positron e^{+} resulting from β+ decay fuses with an electron from patient's tissue and organs, resulting in two anti-parallel direction photons (called gamma rays) with an energy of 511keV. These photon pairs are emitting simultaneously and are detected by the PET scanner. The positron fusing with electron and photons emitting reaction is known as positron annihilation process.

Because a PET scanner should detect all photon pairs emitted by the patient body, the detectors are arranged as a ring surrounding the patient. Only those photon pairs that hit two different detectors on the opposite side of the ring at the same time or in a short predefined timing window[19] are recorded, this being considered as a coincidence event. The predefined time window is called coincidence window and is usually set between 8 to 12 ns. If a sufficient number of coincidences appear (typically 10^{6} to 10^{9} events), it is possible to reconstruct statistically meaning full image of the radiotracer distribution in the patient body[3], [5], [20], [21].

Figure 2.1 illustrates the PET imaging procedure: 1) Radiotracer isotope decay and positron emitting. 2) Positron travelling in the patient tissue then annihilated. 3) Producing two anti-parallel photon rays and4) Each photon hits a detector crystal[22].

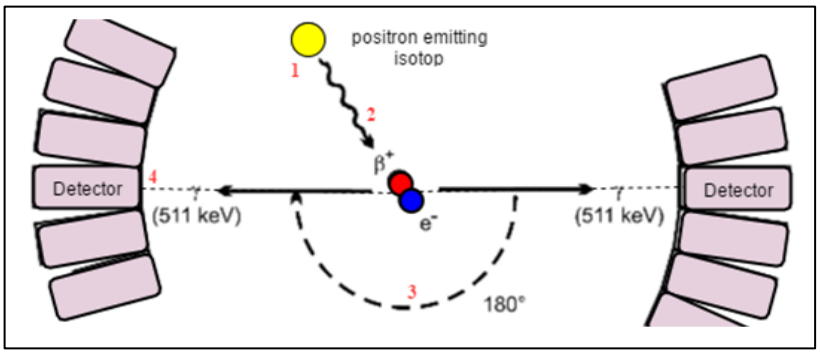

Figure 2.1 PET imaging procedure details

2.3.1 Photon Interaction with Patient's Body

The procedure detailed in the previous section described the ideal PET imaging process and allows the generation of a perfect reconstructing image from a radioactive distribution in the region of interest. In reality, there are other processes can occur at the same time or after annihilation. Consequently, the PET scanner can detect a false coincidence event that leads to image quality degradation.

There are three different types of coincidence events that can be recorded by the PET imaging system as shown in Figure 2.2:

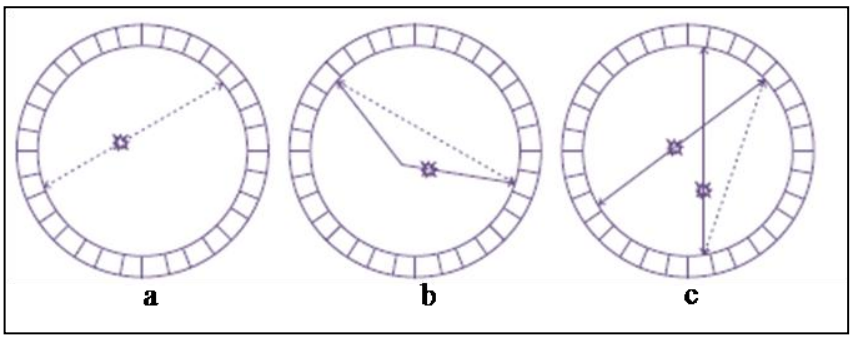

Figure 2.2 Coincidences events

- **True coincidence** (Figure 2.2 a).This event is found when the two detected photons are coming from the same annihilation process. The photons did not interact with the surrounding tissue, so none of them changed its direction, and none of them was scattered.
- **Scattered coincidence** (Figure 2.2 b). This is a true coincidence event but one or both photons interacted with the patient's body before hitting the scanner detector. That mean the photon scattered and changed its direction and arriving at a different detector from the one that is supposed to.
- **Random coincidence** (Figure 2.2 c).This event occurs when two photons from different annihilation processes are hitting two detectors in the same coincidence window.

It is essential to know the amount of each of those events with respect to the total amount of detected coincidence events because valid information about the distribution of radiotracer in the patient's body only comes from the true coincidence, while scatter coincidence provides blur and random coincidence produces noise in the acquisition data.

2.3.2 PET Detectors

As we mention before in section 2.3, the PET system is designed to have a ring of detector blocks. Each block is built from scintillation materials and consists of a collection of small detection elements called crystals as shown in Figure 2.3.

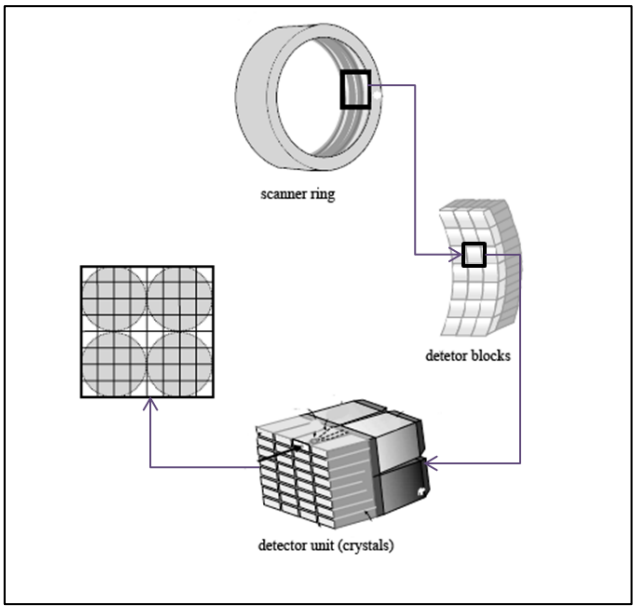

Figure 2.3 PET detectors configuration

Today, the detector blocks build by using two design model either large continues crystals or array of discrete crystals. The first design provides a low-cost detecting system while the other design provides a higher sensitivity system. In either model, the detector blocks arranged as a full ring surrounding patient's body or a partial ring with rotation. Figure 2.4 show the three basic PET scanner configurations found in modern PET systems: a) Array of large detectors block. b) Partial ring of detectors with motion and c) Full ring of desecrate detectors block.

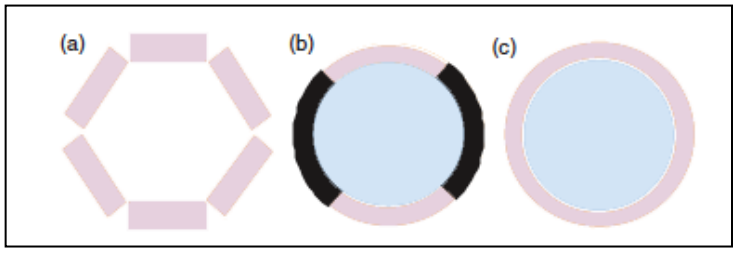

Figure 2.4 PET scanner configuration

In order to work properly and provide the best quality image for a given amount of injected radiotracer, the detector systems must be able to detect all photons with an energy of 511keV that hit the crystals surface. In addition, it should determine when

a photon hits the detector and then, record it and compare the time of all detected events, specifying the photon pair of single annihilation process. Furthermore, it is important to indicate the energy of each resulting photon and to reject the scattered events. Almost all detectors are built with a scintillation material that emits visible or ultraviolet light when it interacts with the emitted photon pairs. The resulting light is detected and converted into electronic pulses using light detectors [23], [24]. The properties should be considered when choosing the detectors materials are efficiency, cost, and physical form. In general, it should be fast, dense and cheap to produce [20], [25]–[27].

2.3.3 PET Acquisition Protocols

There are set of standardized PET acquisition protocols that ensure the stability of the acquired PET data. One of the basic acquisition protocols in PET clinical examination is to collect data over a fixed time. The resulting image represents the average radioactivity concentration in the specific body region during the scan period. This is the typical scanning mode for studies that observe biochemical parameters proportionally to the radiotracer concentration such as studies use the radiotracer of 18F-FDG which remains stables for 30-40 minutes after it is injected [13], [14]. Moreover, the other acquisition protocol requires dynamically following the change of radiotracer concentration for a particular biochemical parameter. The PET data are collected based on a sequence of image frames and the resulting reconstructed image provides information about the biological changes in the radiotracer concentration and distribution over time.

2.3.4 PET Data Representation

The information that gets from projection data acquired by PET imaging procedure is called Line of Response (LOR). The simple approach to storing the information is to organize it into a set of parallel projections called sinogram or histogram. Later, this sinogram should be reconstructed in order to get the image describing the radiotracer distribution within patient's body.

In PET scanner, the LORs are represented as a set of coordinate (s, ϕ), where *s* is the axial distance between LOR and the scanner center while ϕ is the angle of LOR. Figure 2.5 presents the LOR coordinates system [28]

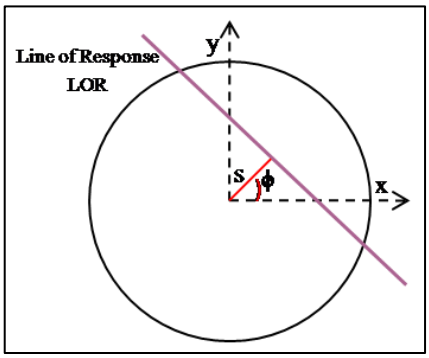

Figure 2.5 The coordinates of the Lines of Response in a Sinogram

A sinogram from a simple PET system can be obtained in two forms: direct and oblique. If all LORs positioned in the same detector ring, the sinogram is called direct sinogram while if they are placed in different rings, the sinogram is oblique. For a scanner system with N detector rings, there are N direct sinogram and N(N-1) oblique sinograms with a total of N^2 sinograms[3].

In a case of direct sinogram ,the radioactivity distribution is a row data consists of detection photon pair events . This data are usually arranged into a 2D matrix that records the number of detecting events for a particular pair of detectors. The matrix is ordered as following: each row represents the projection of the radiotracer activity at a given angle ϕ, and each column represents distance offset from the scanner

center *s*. Equation (2.2) provides the relationship between the elements *s*, ϕ in this matrix for radioactive distribution for an object positioned at the location (x,y) from the center of PET scanner

$$s = x\cos\phi + y\sin\phi \tag{2.2}$$

The sinogram described above is represented in Figure 2.6. The LORs of a point that not cross the scanner center are representing by a curve line on the corresponding sinogram while a point source located in the center is representing by a straight line in the corresponding sinogram[29]–[31].

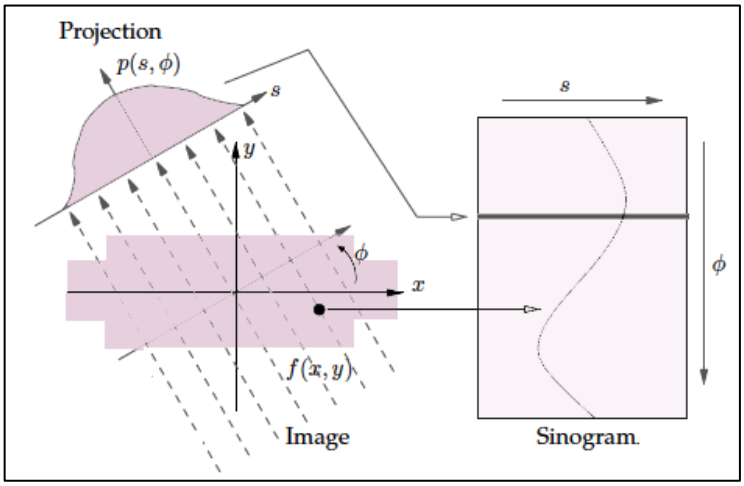

Figure 2.6 A parallel projection, for a specific angle ϕ , of an object corresponds to a row s in the sinogram matrix

2.3.5 PET Image Reconstruction

The radiotracer distribution information stored in the sinogram is very useful but not at a glance. The goal of image reconstruction is to extract from the sinogram a cross-sectional image that illustrates the accurate distribution of the radiotracer in the object being scanned using the mathematical algorithms of the computed tomography. Numerous image reconstruction algorithms have been developed through the years. Two basic approaches for reconstructing image are widely used. The first approach uses mathematical techniques in order to compute the

radioactivity distribution in the scanned object. These algorithms are represented by simple Back Projection (BP) and its extended and improved version, Filter Back Projection (FBP). The second approach is to use statistical techniques in order to find a most reliable image. These algorithms are called iterative algorithms, the ordered subsets expectation maximization algorithm (OSEM) being the most popular.

2.3.5.1 Analytical Reconstruction

Analytical reconstruction algorithms are based on the idea that there is only one possible image can be reconstructed from the given sinogram projections data. The straightforward technique for image reconstruction is simple BP method while the conventional one is based on FBP.

- **Back Projection Method**

As described in section 2.3.4, the radiotracer distribution data in a given LOR in a sinogram represents the count of all photon pairs detected by particular detector pair along a line across the object depth. The method of Simple BP is used to reconstruct the required images from all the LORs stored in a sinogram. The Fourier Slice Theorem supports the principle of BP[5], [32].

For reconstruction an image of a pre-define size, for example,256*256 pixels, The reconstruction image pixel in (x,y) position is related to coordinates in the sinogram data given by equation (2.2) .The measured data in sinogram corresponding to the calculated s is added to the (x,y) position in the reconstructed matrix for all projection angle ϕ . The resulting Back Projected image pixel can be calculated by equation (2.3) where $I'(x,y)$ is the reconstruction matrix , $p(s,\phi)$ is the count of detected event in sinogram and *M* is the number of projection angles.

$$\acute{I}(x,y) = \frac{1}{M}\sum_{M=1}^{M} p(s,\phi) \tag{2.3}$$

$$= \frac{1}{M}\sum_{M=1}^{M} p(x\ cos\ \phi + y\ sin\ \phi, \phi) \tag{2.4}$$

The result of this process is an image that is similar to the true distribution of radioactivity in the given object, but it is also a heavy blurred representation of the object . The blurring of the reconstructed image is directly proportional to the distance of acquired LOR from the scanner center. Thus, the relation between the original radiotracer distribution image I(x,y) and the resulting reconstructed image I′(x,y) can be given by equation (2.5) .

$$\acute{I}(x,y) = I(x,y) \otimes \frac{1}{s} \tag{2.5}$$

The symbol $\otimes$ in the above equation denote the complex relational operation. More information about simple Back Projection reconstruction method can found in[3], [20], [24], [33].

- **Filtered Back Projection Method**

The blurring effect in a reconstructed image introduce by the simple BP can be minimized by applying an image filtering to the PET acquired data. After that, the filtered data is reconstructed by back projected method, the resulting reconstructed image being a representative image of the given object. This technique is called filtered back projection. It is principally based on Fourier transformation method or projection slice theory.

According to the Fourier method, the reconstructed image can be filtered either in the frequency domain (measured projection data p(s,ϕ) in a sinogram) or spatial domain (radiotracer distribution I(x,y) in original object). In this case, the projection data in each LORs is converted from spatial domain to frequency domain. This operation is

known as Fourier transformation while its inverse operation of converting the data from frequency domain to the spatial domain is called inverse Fourier transformation. Equation (2.6) expresses the Fourier back projection reconstruction method.

$$F(v_x, v_y) = FT\ f(x, y) \tag{2.6}$$

In the equation (2.6), $F(v_x,v_y)$ denotes the resulting Fourier transformation of pixel positioning at (x, y) and FT means the Fourier transformation operation. Essentially, the Fourier transformation $F(v_x,v_y)$ of each row in the sinogram is taken and added together.

A more well-designed reconstructing method , named filtered back projection (FBP), be achieved by reformulating equation (2.5) in the spatial and frequency domain. The result is:

$$\grave{F}(v) = H(v) * F(v) \tag{2.7}$$

$\grave{F}(v)$ represents the filtered projection produced from the multiplication of filter function H(v) in the spatial frequency domain and the initial data that is transformed using Fourier transformation F(v). Figure 2.7 illustrates the basic step of reconstructed image filtering.

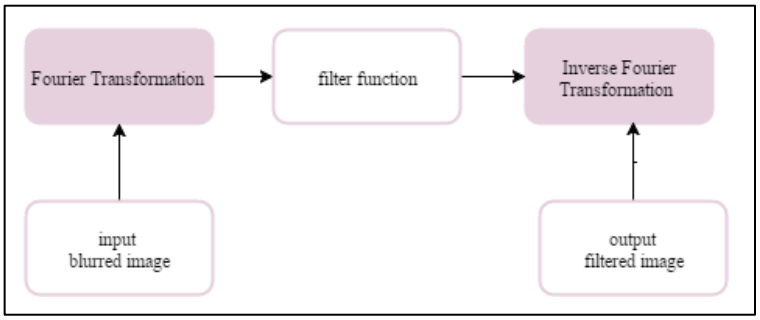

Figure 2.7 Basic step of reconstructed image filtering

The reconstruction filter function is known as the ramp filter which amplifies the high –frequency with respect to the low frequency [9], [20], [24], [34]. FBP gives reasonable results in practical PET reconstruction and its one of the most used reconstruction algorithms. Furthermore, due to its simplicity and to the fact that it is fast in computation, the use of this algorithm is recommended by National Electrical Manufacturers Association NEMA [4], [5], [35].

2.3.5.2 Iterative Reconstruction

Iterative reconstruction algorithms are based on the idea that there is more than one possible image that can be reconstructed from a given sinogram. The main objective of these algorithms is to choose which images looks most like the real object. This is achieved by computing multiple reconstructions and providing an algorithm to choose the optimal image.

Figure 2.8 summarizes the main idea of iterative reconstruction technique. This technology starts by computing an initial estimation of the reconstructed image using analytical reconstruction algorithm, typically FBP. Then, in order to produce a set of estimated projections, the initial reconstructed image is back projected using forward projection method. The estimated projections are compared to the measured projections and, if there is a difference, correction is made to improve the estimated ones. Corrected projections are then back and forward projected again, the resulting projections being compared to the initial ones. The reconstruction processes stop when the difference between estimated and measured projections is reasonable low.

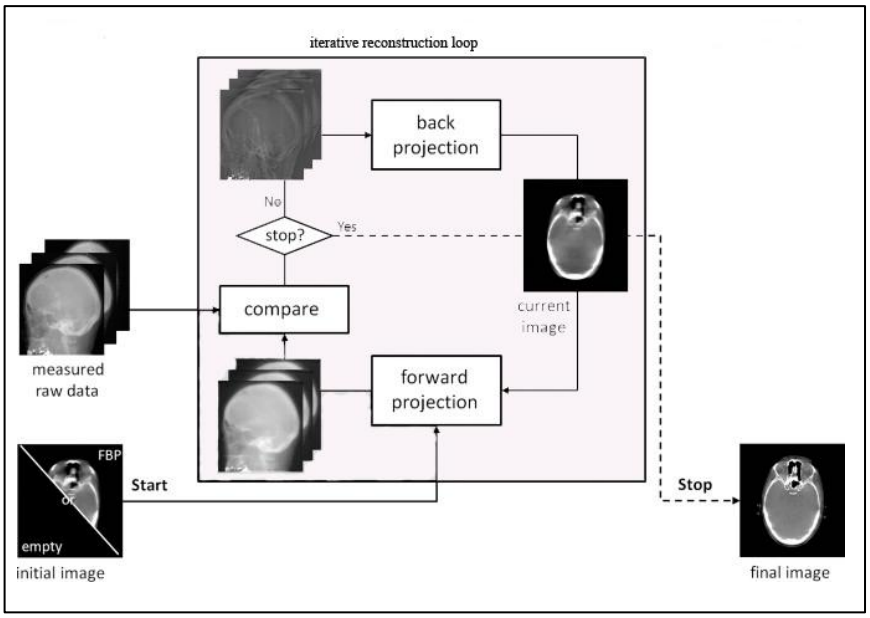

Figure 2.8 Iterative reconstruction technique[36]

An overview on the different iterative reconstruction algorithms can be found in [9], [19], [24], [36], [37]. These algorithms show improvement in reducing noise and provide an image with better quality, but they suffer from some drawbacks such as : computationally slow and requirement of carefully estimated difference parameters.

2.3.6 PET Radiotracers

The radiotracer used in PET imaging can affect the quality of resulting images. All radiotracers used in PET (see Table 2.2) have to satisfy some requirements such as they have to be not toxic or harmful to the patient, they have to be chemically incorporated into the biological process under examination without modifying it. In addition, they should be specific for the physiological process under study, so they have to join specific active molecules and to follow specific ways. Furthermore, they should produce images with low noise and high contrast. The radiotracer molecule has to be easily synthesizable, and it must have a decay time suitable to the clinical

needs. Very short decay time could not be able to detect a sufficient number of coincidence events required to reconstruct the PET acquired image.

Table 2.2 Some radiotracers used in PET imaging and their applications[3]

Radiotracer	Application
2-[F-18]Fluoro-2-deoxy-D-glucose (FDG)	glucose metabolism
[O-15] water, [N-13] ammonia, [O-15] butanol, [O-15] CO2	blood flow
[F-18] Fluoride	bone metabolism
[C-11] O-methylglucose	glucose transport
6-[F-18] Fluoro-L-DOPA	dopamine metabolism
L-[metil-C-11] Methionine	Amino acids metabolism
[C-11] Raclopride, N-[C-11] methylspiperone	dopamine receptors
[C-11] Flumazenil	$GABA_A$ receptors
[F-18] Fluoromisonidazol	ischemia/hypoxia
[C-11] Acetate	Acetate metabolism (Krebs cycle)
8-[F-18] Fluoroganciclovir, 8-[F-18] fluoropenciclovir	genetic expression
8-[F-18] fluoropenciclovir	Inflammation

The most commonly used radiotracer in clinical PET is the glucose analogue ^{18}F-FDG. This is modified glucose compound that acts like normal glucose and allows the imaging of glucose metabolism. As Figure 2.9 illustrates, during the PET examination, FDG is injected into the patient's body, following the physiological pathways to the cells that use glucose as the main source of energy. Then the FDG accumulated and concentrated according to the amount of glucose utilization in each cell. Most of the abnormal tumors and cancer cells consume glucose more than their surrounding normal cells, which makes FDG an effective radiotracer in detecting and staging a variety of cancers. Moreover, this radiotracer became widespread in

everyday clinical routine due to the facts that is easy to produce ,it has an ideal decay time and its able to pass through blood and brain barrier[3], [5].

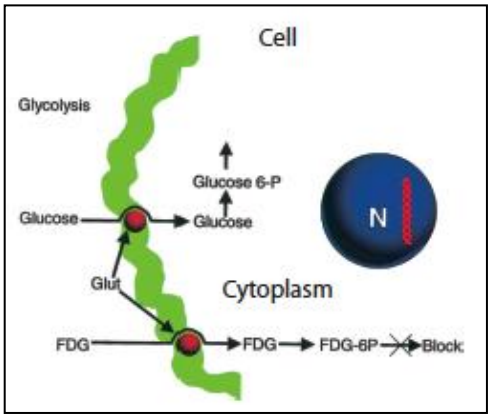

Figure 2.9 FDG radiotracer metabolism in cells[38]

2.3.6.1 Radiotracer Injection Dose

The amount of radiotracer that should be injected into a patient's body is an important issue in PET examination. There are standards on what the dosage amount of radiotracer that must be administrated. In this regard and according to the European Association of Nuclear Medicine EANM , the amount of injected FDG radiotracer applied in the case of whole body scan for adult patient approximately equals to 2.5MBq /kg, when the scan duration equals to 5 min. Alternative recommendations for adult patients scans are given by EANM procedure guidelines [13], [14]. For ^{18}F-FDG whole body PET scan , it is recommended that

$$A = constant * (\frac{m}{70})^{0.8634} \quad (2.8)$$

where *A* denote the amount of administrated radiotracer , *constant* is a factor chosen according to the PET scanner types , *m* is the patient's weight in Kg normalized into weight depend on factor and *0.8634* is the normalization correction[10].

The amount of injected radiotracer is measured as the number of decay per time unit. The common units for expressing radiotracer amount in International System of Units *SI* are Curie (Ci) and Becquerel (Bq). One Ci is defined as $3.7*10^{10}$ decays/second while Bq is defined as 1 decay/second[3].

2.4 Phantom

The purpose of having a phantom or a realistic model of the subject is to represent the patient's body tissue and organ for a region of interest and to allow modelling the radiotracer distribution in a similar manner to real biological tissue and organs. In literature phantom is defined as a mathematical model designed to accurately represents the tissue or the organ system in the whole body [3]. The benefits of using computerized phantoms in medical imaging studies are that the physiological process is monitoring to provides strong bases to evaluate and improve the imaging scanner and devices ,data acquisition methods and image reconstruction algorithms. Furthermore, the computerized phantom can be modified in order to model different test situations. The fundamental designs and technical challenges of computational models for application in a radiological science can be found in[7], [39]–[41].

Computerized phantom can be defined as a simple geometrical structure that consists of mathematical and geometrical shapes like point, line, cylinder, sphere, and disk. This type of phantoms is sufficient for simple device performance evaluation but its fail in reconstruction algorithm evaluation. The other computerized phantom type is voxel based phantom which can provide better representation for the scanner performance evaluation as well as a reconstruction algorithm evaluation under realistic situations. This phantom can be defined from tomographic image segments of the patient, obtained by either CT or MRI acquisitions. In addition, in order to assign the radiotracer activity distribution of different tissues and organs to the

phantom data , some real PET acquisition image may require . This type of phantom is widely used in most dedicated imaging software packages. Because the creation of a voxlized phantom is not straightforward, different standard voxel based phantoms have been developed and available for the simulation studies. Zubal phantom[42] is one of the standard phantoms which provide a 3D model of the structure of an adult male. It is often used for brain simulation studies. In addition, there is another type of phantom representation based on hybrid models. It is defined as a combination of the realistic description of the organ's tissue with flexible mathematical and geometrical representations. One example of this type of phantom is 4D extended cardiac-torso XCAT phantom[43]. It provides a very realistic model of the human structure and their physiological process like cardiac and respiratory motion. The organ shapes are based on CT data and the phantom includes the attenuation coefficients for a given photon energy and for an assigned particular radiotracer concentration value[4]. Figure 2.10 shows an example of two voxlized based phantom sets.

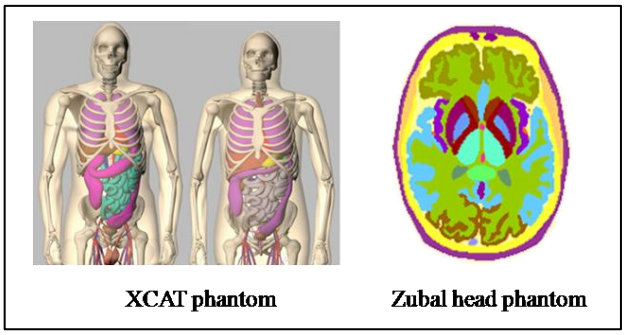

Figure 2.10 Voxlized phantom

2.5 Monte Carlo Method in Emission Tomography

Monte Carlo methods are statistical calculation techniques used to solve problems associated with stochastic processes. The main principle of Monte Carlo methods is to create a model that represents the physical system under investigation. Based on a

random sampling of the prior known probability density functions PDFs of occurrence for each process interaction, the model simulates the processes reaction. This technique has been known since 1770 and it was first applied in field of medical radiation in the 1960s when Anger used it to simulate the physical reaction of a scintillation camera[44]. Since then, due to the stochastic nature of radiation processes such as emission, transportation, and detection ,Monte Carlo method has become a very popular simulation technique in the field of nuclear medicine.

Actually, the Monte Carlo simulation technique plays an essential role in nuclear medicine researches and studies [6]. It is useful to understanding the concepts of imaging systems like PET, quantifying the radiation amounts, planning the radiotracer dosage, measuring the performance of new-modelled scanner, as well as optimizing its design and protocol. Nowadays, the simulation data is important for the assessment of image reconstruction algorithms development, evaluation, and validation .The main advantage of this simulation method in nuclear medicine and particularly in PET imaging is the possibility to change different parameters during the simulation scenario, which allows to investigate and evaluate the effect of those modifications on the system performance. Usually, this is impossible or too expensive to test using a real experiment or analytical calculating approaches.

In the context of nuclear imaging field, the success of the Monte Carlo technique is related to its ability to describe the physics of particles interaction with material based on the random generator, and to its ability to model rules that describes the interaction of particle movement through materials by using particle cross section and sample probability distributions. In photon tracking simulation, the data of cross section provide information used to calculate the length of photon path and the interaction type. After that, using random number generators and prior known rules

for sampling, the PDFs of the photon events are sampled. The energy of that photon may be wasted during its path or it can pass throw all materials until it reaches the detector. Later, the PDF sampling makes the decision whether the tracked photon should be accepted or rejected[6], [44].

The main components of Monte Carlo simulation applied to PET imaging system illustrated in Figure 2.11 are:

- **Random Number Generator**

Random numbers and Random Number Generators (RNG) are important for modelling physical systems having a stochastic nature. The RNG should create a sequence of numbers in long runs within a short time period. The resulting sequence has to be uniform, uncorrelated and reproducible. A computerized RNG algorithm delivers the sequence of numbers based on a fixed number known as seed. Linear Congruential algorithm is one of the most common RNG algorithms which use equation (2.9) to generates its seed

$$S_{n+1} = (aS_n + b) mod(2^m) \tag{2.9}$$

Where *a* and *b* are constant integers, *m* is a computer word size. The seed number is randomly changed by using values from the computer's system clock [45].

- **Sampling Method**

It is a practice to obtain statistical variables that are distributed according to a particular probability distribution function PDF. The based method of sampling for Monte Carlo simulation was developed in the Manhattan Project and published by Von Neumann in 1950s. Nowadays, different sampling techniques are available: distribution sampling, rejection sampling and mixed sampling techniques. With the distribution sampling technique a cumulative distribution function CDF(x) is

generated from the integral of probability distributions PD(x) over a specific interval [a,x] as in equation (2.10).

$$CPD(x) = \int_{a}^{x} PD(x')dx' \tag{2.10}$$

In order to sample the x variable, the CPD(x) is replaced with a random number from the uniform distribution over range of {0,1}. [6], [41]

- **Photon Transport**

One of the most important physical interactions in nuclear medicine imaging simulation is the photo-electric effect. The total cross section data for a given photon in specific energy E can be calculated by interpolating the discretized libraries. The photon incident is absorbing and emitting an electron which has the same direction as its original incident photon. The electron energy is defined as the incident photon's energy minus the electron binding energy. For all emission events, the photon emission is randomly and repeatedly sampled across the total and partial cross sectional data.

- **Variance Reduction**

This makes a simulation statistically efficient. This is achieved by obtaining a high precision of estimated number of iteration and by obtaining smaller time to compute number of events at single detector. For more details see[6], [41], [46], [47]

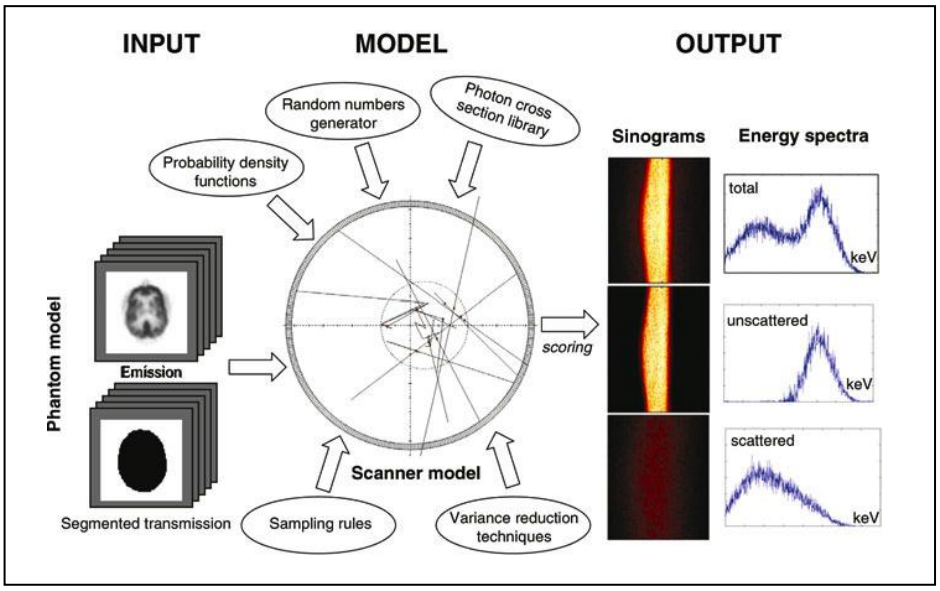

Figure 2.11 Monte Carlo simulation applied to PET imaging system from[9]

More details of the principles and main components of Monte Carlo simulation in medical applications can be found in [6]–[9], [41], [45].

2.5.1 Monte Carlo Simulations Software

Several Monte Carlo codes for simulating a wide range of emission tomographic studies were developed over last dedicates. Those codes can be classified into two main categories: analytical code and practical tracking code .In addition ,the particle tracing code category is divided into general purpose code and emission tomographic dedicated code. The general purpose codes are usually used for high energy particles while the dedicated is developed specially for SPECT or PET simulations [3]–[5], [44]. The most popular general purpose codes are: the Electron Gamma Shower (EGS) code [48], the Monte Carlo N-Particle (MCNP) transport code [49], the GEometry ANd Tracking (Geant) toolkit[50], and the Code System to Perform Monte Carlo Simulation of Electron Gamma-Ray Showers in Arbitrary Materials (PENELOPE)[51]. The available emission tomographic dedicated codes are: Simulation System for Emission Tomography SimSET [52] and the Geant4

Application for Emission Tomography GATE[53]. All of these codes suffer from multiple drawbacks and limitations in terms of speed and difficulty of use ,but they are advantageous in terms of validation and support.

Recently, the most powerful dedicated code enabling PET simulation is GATE. This Monte Carlo based simulation. The leading drawback of this code is the extremely high simulation time. For example, to simulate a scan of the whole body, more than 17000h CPU time is required. The photon detection efficiency is the second limitation because detection efficiency becomes much small when the simulation has a large number of particles. Furthermore, the complexity and hard programming skill necessary to use it are other limitations. The user needs to carefully specify all details of the simulated processes and it is difficult to adapt the specific needs according to the simulation requirement. For that reasons, self-made Monte Carlo based simulation may be refereed for overcoming the public code limitations and achieve the desired goal. This is especially true in case of seeking simplicity of use with a high execution time[4], [44], [54].

For comprehensive overview of the Monte Carlo simulations software package, go to [41], [44], [55], [56].

3 METHODOLGY

CHAPTER III

METHODOLGY

3.1 Introduction

In this chapter, we describe the significant steps to simulate the PET physical operations and discuss the proposed methodology for predicting the radiotracer-injected dosage for adult patients by optimizing the dosage recommendation amount used today in the clinical examination in order to detect abnormal lesions and tumors. As shown in Figure 3.1, any computerized PET imaging system is composed of phantom specifications (patient model) and scanner specifications, processed by simulation software in order to reconstruct the PET desired images.

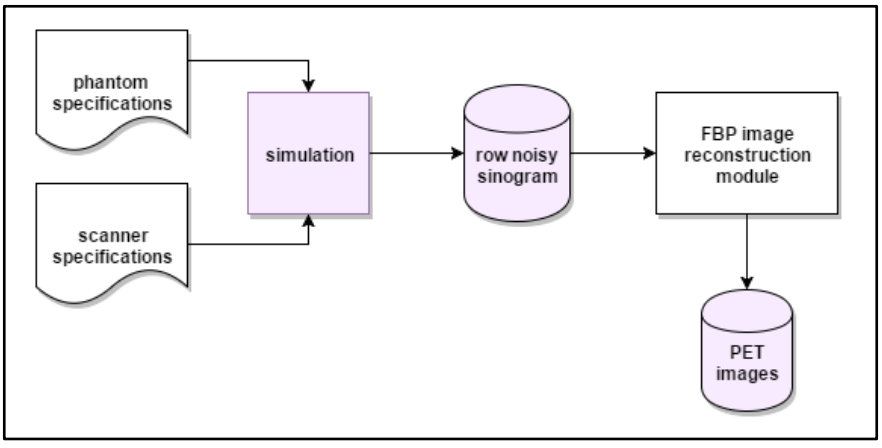

Figure 3.1 PET simulation basic structure

Phantoms are seen as a collection of digital volume arrays (2D images) that are used to approximate the locations and dimensions of the patient's body structures and

organs. These phantoms are mainly derived from segments of CT or MRI tomographic images of the required part of the patient's body. A scanner model designed to illustrate a common cylindrical PET scanner currently used for clinical patient examinations. It models important parameters of the scanner: detectors material, detectors surface area (mm^2),detectors diameter ring (mm), a number of detector rings, and a number of detectors per ring. The process of PET imaging is then simulated based on the Monte Carlo method. For simulation implementation, we follow the basic algorithm provided in [57] . The algorithm covers PET processes like radiotracer activity uptake, acquisition time, positron range, positron inhalation, photon transportation, and photon detection. The information that come from the simulation are organized in a matrix called sinogram. Sinogram is a simply ordered way to store the events registered by each detector into sets of parallel projections. Finally, we reconstruct the PET image of the injected radiotracer activity distribution within required part of patient's body.

In order to produce a PET hybrid image that shows the functional information about the activity distribution as well as the anatomical information, we combined the resulting PET image with CT or MRI tomographic images by investigating an image fusion function.

The details of implementing all of above processes is presented and discussed in the following sections.

3.2 Patient Model

Generating a realistic model of the patient's anatomical and biological functions from imaging data is the important aspect of simulation [7], [9], [40]. Theoretically, the patient computerized model represents a tissue, organs and body region in order to visualize the radiotracer distribution, scattering and absorbing as similar as in real

patient. By using a computerized model of the patient, we were able to test different or completely innovative cases by simply altering that model with different situations.

3.2.1 The Phantom

As shown in Figure 3.2, two digital volumes were used for the Monte Carlo simulation performed: a matrix generated from reading a real clinical data and a matrix of the digital anthropomorphic phantom.

The PET examination scenario simulated in this work is very closed to a real examination scenario. Clinical data provides the approximate accurate experimental results, while digital phantom provides the simulation data for evaluation of detecting abnormal lesions and tumors.

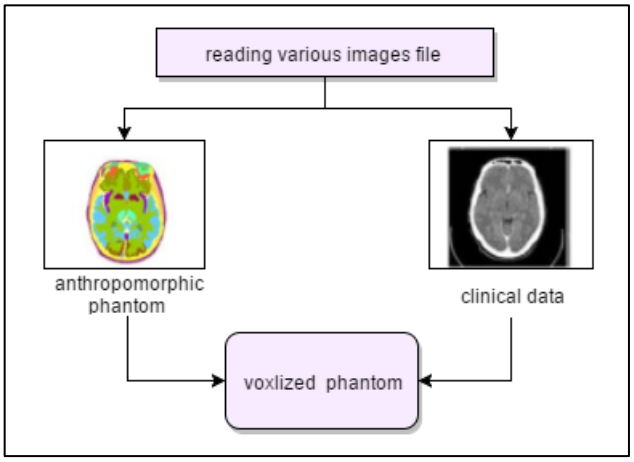

Figure 3.2 Digital voxlized phantom

3.2.2 Phantom Builds from Real Data

The generation of realistic patient's phantom from real data generated two different maps represented as array: 1) a map of radiotracer distribution in the patient tissue and organs called emission map; 2)a map of the photon travelling and absorption

through the patient body structures (this map is called an attenuation coefficient map and plays a vital part in representing a more accurate phantom).

Regarding the radiotracer activity used in the simulations presented in our experimental examination (^{18}F-FDG), the values presented in emission maps were developed using image-based segmentation in AMIDE software[58] and scanning scenario was done using realistic software simSET [52]

3.2.3 Radiotracer Injection Dose Calculation

According to EANM guideline recommendation for ^{18}F-FDG PET examination ,there is standard recommendation on radiotracer amount injected to the patient(IA) [14]:

$$IA = 7.2 * patient\ weight(KG)/scan\ time\ (min) \pm 10 \quad (3.1)$$

By flowing the principle of as low as reasonable achievable (ALARA) [18], each patient should receive the minimum amount of IA that is necessary to produce a good diagnostic image. To this purpose and along with the variation in patient body parameters, we proposed a method to scale the IA dose according to patient's age based on EANM guideline recommendation and Young's formula used in nuclear medicine dosage calculation[59]–[61] :

$$\mathrm{IA}' = \left[\frac{\text{patient age (year)}}{\text{patient age(year)} + 12}\right] * \mathrm{IA} \quad (3.2)$$

The details of calculating IA' method is described in the following flowchart in Figure 3.3:

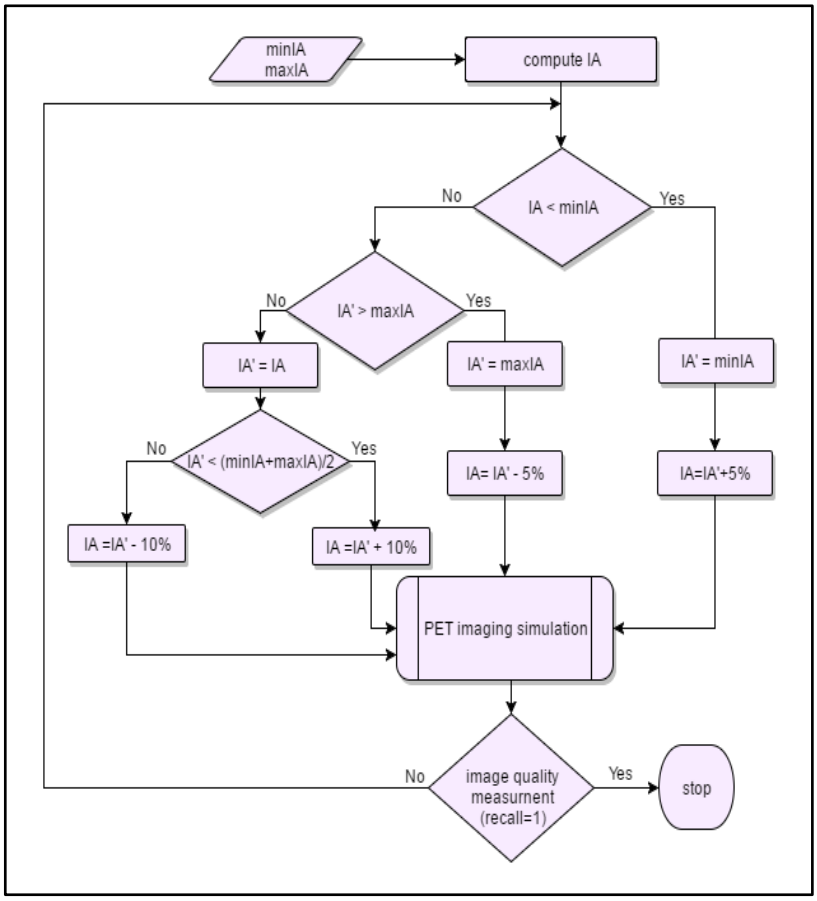

Figure 3.3 Radiotracer injection dose calculation process

3.2.4 Phantom Simulation Process

Using MATLAB platform, the phantom data is read as a binary file and arranged into a reshaped array having the following dimensions: data-dimension*data-dimension*data-size. According to the digital phantom set used in the current study, the array size is 256*256*128. The next step consists in forming the radioactivity distribution map (emission map) as a matrix based on the table of activity distribution ratio coming from simSET scanning for the ^{18}F-FDG.Then, the matrix of attenuation coefficient map is formed by following the same strategies applied in the emission map forming. The constant linear attenuation coefficient (μ) of the approximated organs and structures is calculating using simSET based on the phantom geometry and the photon travelling distance. The different attenuation

coefficient (μ) of the structures is approximated with our constructed phantom illustrated in Table 3.1.

Table 3.1 Example of attenuation coefficient of the structures in Zubal phantom

Tissue and structure	Linear Attenuation Coefficient (μ)
Pons	0.528
Gray matter	0.212
White matter	0.213
Cerebrospinal fluid	0.207
Water	0.206
Fat	0.185
Air	0.0004

An example of the activity distribution table for ^{18}F-FDG radiotracer activity in the phantom under study is showed in figure 3.4. The first two columns in the activity distribution tables define the index intervals of organ and tissue, e.g. {0,82} in the first line of figure 3.4 while the third column attached a correlated activity ratio ,0 in this example . In a case of the Zubal phantom, each organ and tissue are associated with specific indexes that make clear implementation of emission map and attenuation map .Table 3.2 contains 24 out of the 63 Zubal phantom index numbers and their corresponding information about structures and organs of interest.

Table 3.2 Index numbers and their associated structures in Phantom under study

83	white matter	101	caudate nucleus	113	cerebral falx
85	medulla oblongata	103	insula cortex	114	temporal lobes
88	artificial lesion	105	Putamen	115	fourth ventricle
89	frontal lobes	107	internal capsule	117	parietal lobes
91	Pons	108	septum pellucidum	120	globus pallidus
95	occipital lobes	109	Thalamus	122	cerebral aqueduct
96	Hippocampus	111	corpus collosum	123	lateral ventricles
98	Fat	112	special frontal lobes	124	prefrontal lobes

```
################################################################################
#   INDEX TRANSLATION FILE FOR THE PHG SIMULATION ACTIVITY INDEXES TO
#   ACTIVITY TABLE ENTRIES.
#
#   This is set up to be a rough simulation of FDG distribution in an oncology study.
#   Brain concentration is set to 4,  and everywhere else to 1. Outside the brain is zero.
#
#       The format of the file
#       Zubal tissue index interval         required activity concentration
#
################################################################################
0   82  0
83  83  1
84  84  0
85  85  4
86  87  0
88  88  5
89  89  4
90  90  0
91  91  1
92  94  0
95  97  4
98  100 0
101 103 4
104 104 0
105 108 1
109 109 4
110 110 0
111 111 1
112 114 4
115 115 1
116 116 0
117 117 4
118 119 0
120 120 4
121 121 0
122 123 1
124 124 4
```

Figure 3.4 SimSET activity distribution table for ^{18}F-FDG radiotracer activity in Zubal phantom

3.2.4.1 Adding Tumors and Lesions

At this step, we will define one or multiple tumors on a particular phantom. A tumor area is a rectangular of Gaussian nature, the radioactivity distribution using equation (3.3). In this equation *IA* represents the total injected activity computed the previously in section 3.2.3., *AM* of specific point is the radioactivity distribution ratio getting from emission map constructed in previous step, *x, y* represent the boundaries of the tumor area, and σ is the variance of that values.

$$tumourActivity = (IA - AM_{x,y}) * exp(-\left[\left(\frac{x - x_0}{2\sigma_x}\right) + \left(\frac{y - y_0}{2\sigma_y}\right)\right]) \quad (3.3)$$

In order to match the radioactive distribution ratio of the surrounding healthy tissue, the radioactive distribution ratio is set as the higher value at the center of the tumor area and is gradually reduced towards the edge of the tumor. We can specify more than one tumor of different sizes at different positions in single phantom.

3.3 Scanner Model

When defining the model of a tomographic scanner, specific guidelines with respect to the hierarchy of the scanner component must be followed in order to track the particle's physical interactions. Most PET scanners are built from single or multiple rings, each ring having several blocks divided into crystal detectors.

In order to provide a basic building block for the scanning experiment, here, we are using a novel tomographic scanner model. In addition to specifying the number of scanner rings, we are required to specify the radius of each ring and the surface area for a single crystal detector. The number of crystal detectors in blocks for single ring computing as following:

$$No.Detectors = \frac{2\pi * RingRadius}{DetectorSurfaceArea} \quad (3.4)$$

According to[34], the ring radius is usually setting between 300 and 600mm and the surface area of each crystal detector is usually setting between 2 and 5mm.

3.4 PET Process Simulation

After setting up the scanner model, we define the PET physical processes that occur during the simulation. The four processes we implementing are summarize in the next illustrating chart (Figure 3.5).

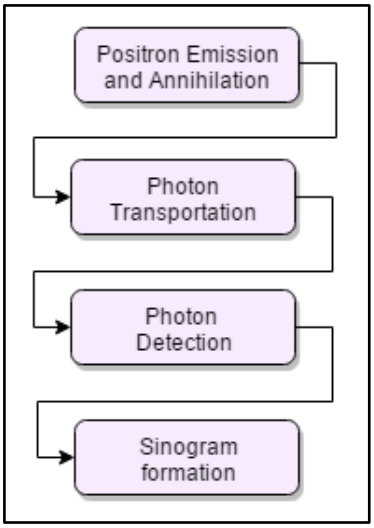

Figure 3.5 PET physical processes implementing in the simulation

3.4.1 Positron Emission and Annihilation

Through the process of radiotracer decay and before the process of annihilation, a positron is emitting and comes out from the radiotracer nucleus with a certain energy. This positron travels some distance inside the patient's tissue until it loses its energy (principally due to the Coulomb interactions with the surrounding electrons) [24]. Then, the annihilation process between this positron and one electron happens. The distance from the emission point to the annihilation point is called positron range. For ^{18}F-FDG radiotracer, the positron range has a maximum value of 2.3mm

and an average value of 0.16 in water phantom[62], [63]. As in [62] the range is distributed as screwed function and when the event number is large, it can be treated as Gaussian function. The positron range distribution of ^{18}F-FDG in water phantom simulated by[64], [65] is present in Figure 3.6

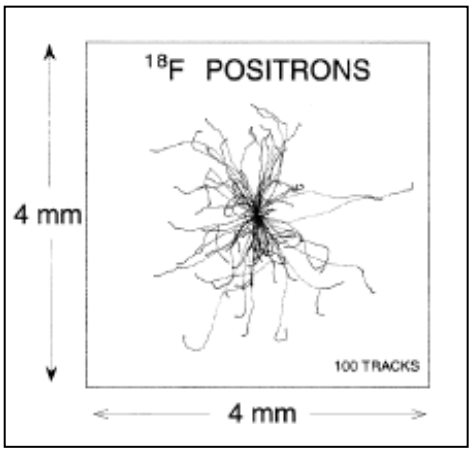

Figure 3.6 positron range for ^{18}F-FDG in water, adapted from [65]

In this work, we will randomize the positron range (PR) by applying a method of generating exponential variate based on basic method for pseudo-random number sampling, known as inverse transformation sampling. For implementation, we define an array of pseudo-random number generated from uniform distribution UD in the {0,1} interval. The exponential variate of the PR is computed as in equation (3.5). In order to insure that the positron distribution range PR is not exceeding the maximum value of 2.3 and is not lower than 0.0,we use the inverse cumulative distribution function F^{-1}[66] .

$$PR = F^{-1}(UD) \tag{3.5}$$

As mentioned in[66], [67], the inverse cumulative distribution function F^{-1} is calculated using the equation (3.6).

$$F^{-1}(UD) = \frac{-\log(1-UD)}{\lambda} \tag{3.6}$$

For $\lambda > 0$, λ is a distribution parameter that defines the random events occurrence and it is known as intensity parameter. Because UD is a uniform distribution in the {0,1}

interval, (1-UD) is distributed as UD[68]. This means that the exponential variate of PR in equation (3.5) is generated as follows:

$$PR = \frac{-\log(UD)}{\lambda} \tag{3.7}$$

Moreover, when PR reaches a maximum value of 2.3, the random events distribution is becoming 0, the distribution parameter is set to $\lambda = 10$ and the equation (3.7) is updated. The final positron range PR calculation equation implemented in our simulation in order to randomize PR is based on equation (3.8):

$$PR = -0.23 * \log(UD) \tag{3.8}$$

By using equation (3.8), we ensure that the simulation is randomly selecting range for each positron emission PR within our limited interval. The generated value of PR is used in the next step to determine the coordinates of the annihilation point.

3.4.1.1 Positron Emission Direction

After choosing the emission range, we will randomly choose a direction for each emitted positron. This positron can go in any direction within angle θ between 0° to 360°.The direction angle θ is randomly generated using RNG by selecting a number from the uniform distributed numbers in the interval {-1,1}.Then we set the selected number to be the cosine value of the direction angle θ, cosθ.

3.4.1.2 Positron Annihilation Point Coordination

We consider the coordinate of the point where the positron is emitted as (PE_x,PE_y) and the final point where positron is annihilated with the electron as (PA_x ,PA_y). The x-coordinate PA_x and y-coordinate PA_y of positron annihilation point for direction angle θ between 0° to 180° with $\sin\theta \geq 0$ [57] and random generated number between 0 and +1 are computed using the following equations:

$$PA_x = PE_x + PR * \cos\theta \quad (3.9)$$

$$PA_y = PE_y + PR * \sin\theta \quad (3.10)$$

In order to expand the angle range from 0° -180° to 0°-360°, we computed the coordinates of the annihilation point which lays between 180° -360° based on a random generated number between -1 to 0 and $\sin\theta < 0$:

$$PA_x = PE_x + PR * \cos\theta \quad (3.11)$$

$$PA_y = PE_y - PR * \sin\theta \quad (3.12)$$

At the end of the above steps, we ensure that all possible direction of emitted positron are computed and that the annihilation point for the ^{18}F-FDG positron emission range {0-2.3} is identified.

3.4.2 Photon Transportation

As mentioned in chapter 2, the results of positron and electron annihilation process are two photons. Those photons are transported through the patient's tissue until they hit the scanners detectors. In this step, we track the movement direction of the generating photons assuming that photons are moving exactly 180° away from each other at any direction.

The angle of the photon movement (transportation line) is randomly chosen using the same steps followed in section 3.4.1.1 for the positron emission direction. In addition, we are identifying the (X,Y) coordinates of one point laying on the photon transportation line by following the same procedure described in section 3.4.1.2.

By determining the coordinates of the annihilation point (PA_x ,PA_y) and the coordinates of the point on the photon line (X ,Y), the photon transportation line slop *m* can be computed as :

$$Y = m\,(X - PA_x + PA_y) \quad (3.13)$$

3.4.3 Photon Detection

The PET scanner used in this work (as described in section 3.3) is based on ring of detectors. We set the coordinate of the ring center point as (R, R) where R is equals to the radius of the same ring. Then, this ring of detectors can be described mathematically by the equation:

$$(X - R)^2 + (Y - R)^2 = R^2 \tag{3.14}$$

From the equations (3.11) and (3.14), the coordinates of the ring detector crystals (PD_x,PD_y) (the point in the detector that the photon ray hit)can be calculated as:

$$PD_x = \frac{-2(2PA_y - mPA_x - 2R) \pm \sqrt{4(PA_y - mPA_x - 2A)^2 - 2(PA_y - mPA_x - 2A)^2(1 + m^2)}}{2(1 + m^2)} \tag{3.15}$$

$$PD_y = m(PD_x - PA_x) + PA_y \tag{3.16}$$

We have two photons from each annihilation processes, two detection point are generated and the result of above equation is always greater than zero. In next section, the sinogram is built by randomly choosing one of those two points.

3.4.4 Sinogram Formation

The sinogram is only information obtained from the positron emission tracking. As defined by [57] , the ultimate meaning of the sinogram is “how many photons hit the certain detector in the certain angle”.

While the coordinates for annihilation point and detection point beside center point of the detectors ring are already computed from the previous stages. In this step, we compute the value of the angle α between the photon transportation line and the detector line of response LOR (the connection line between photon detection point on the scanner ring and the detector ring center point), as shown in the Figure 3.7.

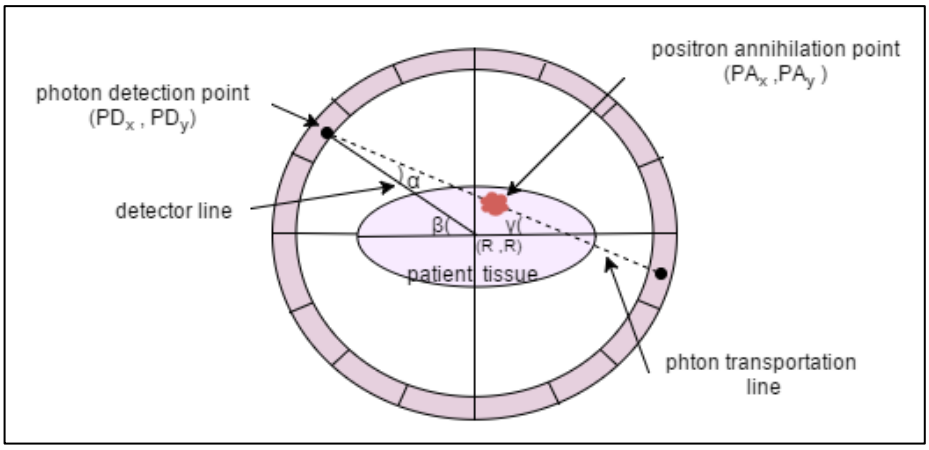

Figure 3.7 Sinogram building process

In addition to the α angle, Figure3.7 illustrates the existence of angles β and γ which represent the angle formed by detector line of response LOR and the angle formed by the photon transportation line respectively. The value of α can be easily calculated by determining the tangent values of those two angles β and γ which equals to the slope value of its corresponding line.

$$\tan\gamma = \frac{PD_y - PA_y}{PD_x - PA_y} \tag{3.17}$$

$$\tan\beta = \frac{PD_y - R}{PD_x - R} \tag{3.18}$$

From the Pythagorean theorem[69], the value of α is calculated as following:

$$(\tan\alpha)^2 = (\tan\gamma)^2 - (\tan\beta)^2 \tag{3.19}$$

$$(\tan\alpha)^2 = (\frac{\tan\gamma - \tan\beta}{1 * \tan\gamma * \tan\beta})^2 \tag{3.20}$$

$$\alpha = \pm\arctan(\frac{\tan\gamma - \tan\beta}{1 * \tan\gamma * \tan\beta}) \tag{3.21}$$

Then the value of α is set to positive if the photon transportation line goes anti-clockwise from the LOR, otherwise is set to be negative. We will repeat this process for all detectors positioned at the scanner ring.

3.4.4.1 Sinogram Building Process

Now, we are going to build a sinogram matrix and fill it using the certain angle β to decide which detector element is hitting with a particular photon in each coincidence event. In order to perform this aspect, the following steps are done. First, using equation (3.4), we compute the total number of detector elements (crystals) in the scanner ring that form the specific angle β.

$$ND = \frac{2\pi * R}{DSA} \tag{3.22}$$

Where ND is the number of detecting elements, R is the ring radius and DSA is the size of each detecting crystal and its setting at scanner modelling stage.

Next, we divide the entire scanning ring into ND parts. Each part forms its own β angle in combination with the detector line LOR. Then, the ring parts are arranged into four equal quadrants. For each photon event, we first find the quadrant of detector and then, the angle β is used to determine the detector crystal number (as shown in Table 3.3). After that, we repeat all of those steps for all generated two opposite photons (photon pairs) and we complete the sinogram matrix by adding one to the point (detector number, α).

Finally, using this procedure, we are satisfying the definition mentioned at the beginning of this section. Consequently, we are determining how many photons-pair hit the certain detector (using β angle) at a certain angle (as α angle).

Table 3.3 Detectors ring arrangement

Quadrant	Detector number
First quadrant	β* ND / 360˚
Second quadrant	(180˚-β)* ND / 360˚
Third quadrant	(180˚+β)*ND/ 360˚
Forth quadrant	(360˚-β)*ND/ 360˚

*ND = total number of detecting elements

3.5 PET Image Reconstruction

In sinogram matrix built in section 3.4, we have saved two key parameters: the number of excited crystal detector (the detector that the photon hit) and the angle α between photon transportation line and the detector line of response LOR. From these parameters, we reconstruct the PET image using the filter back projection FBP reconstructing algorithm .Due to its simplicity and fast computational process, FBP is a recommended algorithm by National Electrical Manufacturers Association NEMA[5] To achieve the desired PET image, we implement the reconstruction algorithm provided by [57] as follows. First, the angle θ for each detector crystal is calculated by comparing the list of detectors to the total number of detector ND already defined in the pervious stage using equation (3.22).

$$\theta = 360° * \frac{detectorNo.}{ND} \tag{3.23}$$

Then the coordinates of each detector (D_x,D_y) placed in the scanner ring can be determined using the angle θ and the equation(3.14).When $0 \leq \theta \leq 180^{\circ}$ then the detector coordinates are:

$$\begin{cases} D_x = R - \sin\theta & if \quad \theta \leq 90^{\circ} \\ D_x = R + \sin(\theta - 90°) & if \quad 90^{\circ} \leq \theta \leq 180^{\circ} \end{cases} \tag{3.24}$$

$$D_y = R - R^2 - (D_x - R)^2 \tag{3.25}$$

If $180^{\circ} \leq \theta \leq 360^{\circ}$ then the detector coordinates are:

$$\begin{cases} D_x = 2R - \sin(\theta - 180°)\, if \quad 180^{\circ} \leq \theta \leq 270^{\circ} \\ D_x = R - \sin(360° - \theta\,) \quad if \quad 270^{\circ} \leq \theta \leq 360^{\circ} \end{cases} \tag{3.26}$$

$$D_y = R + R^2 - (D_x - R)^2 \tag{3.27}$$

Now, in order to recognize all spot positioned on the photon transaction line ,we calculate the slope m_p of each photon line using (D_x,$D_{y)}$ coordinates and the angle α taking from the sinogram as in following equations :

$$\begin{cases} m_p = \tan\theta + \alpha & if \quad \alpha \leq 0^{\circ} \\ m_p = tan\,\theta - \alpha & if \quad \alpha \geq 0^{\circ} \end{cases} \tag{3.28}$$

After that, the number of events already stored on sinogram matrix field (detector number, α) is added to the recognized spots, as shown in Figure 3.8.

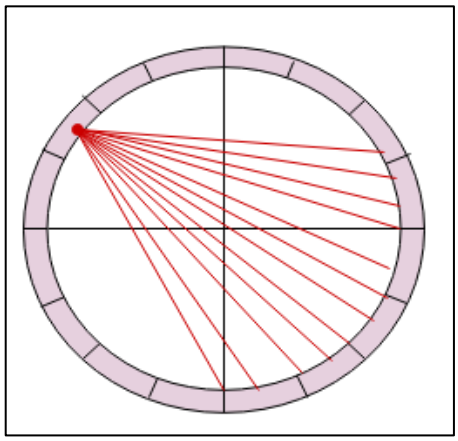

Figure 3.8 Reconstruction of single detector crystal

Finally, by repeating the above procedure for every crystal in the detector block, the PET image can drown.

3.5.1.1 Fusion of the PET Reconstructed Image

In this step, in order to provide a combination image of PET /CT or PET /MRI which is used mainly for getting more accurate diagnoses information by enhancing the details of information from the obtaining image, we align the resulting constructed image with the CT/MRI image used for phantom building [70]. The fusion procedure is performed as follows: After the PET image is reconstructed and the filtering is applied to the resulting image. The next step is performing a spatial transformation between the two images one of the PET and other of CT or MRI. The key of the spatial transformation step is to align the two images by defining a spatial relationship between the pixels of one image and relocating them into a new location in the resulting image. The final step in image fusion is the overlapping of the two images with a suitable level of transparency.

3.6 Image Quality Assessment

There are many image quality assessments tools available in the field of PET reconstructed image expressing and evaluation. For the purpose of our work, we are choosing to evaluate the two most popular tools: Signal to Noise Ratio (SNR) and Noise Equivalent Count (NEC).

Furthermore, because from the medical point of view, for a given diagnostic task such as tumor/lesion detection, the significant measure for PET image quality is observing and detecting small foci [10], [15], we provide a particularly attractive performance measurement of the reconstructed image precision and recall.

3.6.1 Signal to Noise Ratio

SNR is a statistical measurement representing the relation between an acquired signal and the background image noise. We are getting its value by calculating the ratio of total detected photons mean DP_{μ} to the signal standard deviation DP_{σ}.

The total detected photons DP is computed by counting all detected events at each detector crystals for all detecting blocks of the scanner ring. Then, by taking the square root of detected photons mean DP_{μ} we can calculate the standard deviation DP_{σ}. The SNR is a decibel logarithmic parameter, and it is calculating by equation (3.29).

$$SNR = 20\ \log(\frac{DP\mu}{DP\sigma}) \tag{3.29}$$

3.6.2 Noise Equivalent Count

NEC is a statistical measurement describing the number of detected photons needed to produce an equivalent image with PET ideal system. It is obtained by calculating

the ratio between the numbers of detected photon DP to the total number of photon events[10], [12], [15].

$$NEC = \frac{T^2}{T + S + R} \tag{3.30}$$

where T is the true event (detected photon event), S is scattered event and R is a random event (S and R are undetected photon events).

In cylindrical PET systems, NEC is directly proportional to the square of SNR [12], [71] and it can to be evaluated as following:

$$NEC = \left(20\ \log(\frac{DP\mu}{DP\sigma})\right)^2 \tag{3.31}$$

3.6.3 Performance Measurement

As stated before, the ultimate measure of PET image quality is the ability to detect the presence of possible tumors and lesions. In a certain situation, the PET image is regarded as the realization of a tumor sampling on a specific region. The diagnostic task of classifying significant changes of pixel values of the reconstructed image according to the given region can be treated as a problem of tumor detection and location.

There are several measures of performance for the tumor detecting classifiers such as precision and recall. In order to calculate precision and recall, the classifier confusion matrix is computed. As shown in Figure 3.9, confusion matrix is a composite of four elements: True Positive (TP), True Negative (TN), False Positive (FP), and False Negative(FN) [72]–[74] . For each pixels associated with tumor values in the reconstructed image, we have a true result if the detected and true classes are the same. TP indicates how many tumors-pixels are detected as tumor and accepted while TN indicates how many not-tumors-pixels are detected as not-tumor and

rejected. The error occurred when the detected class and true class are opposite. In this situation, FN indicates how many tumor-pixels recognized as not-tumor and FP indicates how many not-tumor-pixels are detected as tumor-pixel

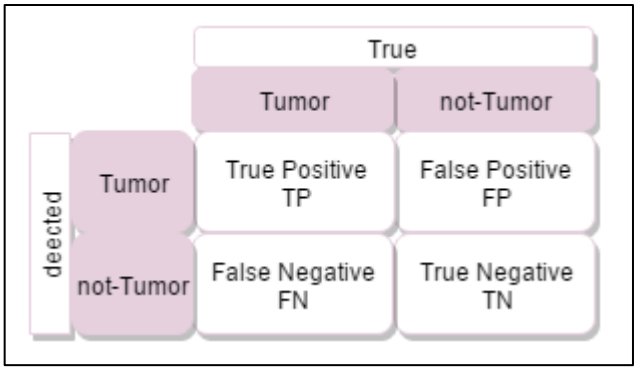

Figure 3.9 Confusion matrix

Precision measures the percentage of the pixels detected as tumors that are truly tumors. Recall measures the percentage of tumor-pixels that are truly detected from all pixels in the reconstructed image. The following equations represent the precision and recall, computed based on the confusion matrix:

$$precision = \frac{TP}{TP + FP} \tag{3.32}$$

$$recall = \frac{TP}{TP + FN} \tag{3.33}$$

4 RESULTS

CHAPTER IV

RESULTS

4.1 Introduction

In this chapter, different simulations on a set of patient chosen from clinical data are performed. We have 60 patients MRI images and metadata from available open source Digital Imaging and Communication in Medicine DICOM library. The main purpose of these simulations is to evaluate the simulated PET system discussed in previous chapters and then predict the optimal radiotracer injection dosage used in detecting abnormal lesions and tumors. .

4.2 Technical Requirements

The simulations in this study are performed using MATLAB R2013a (win32) on a Windows7 operating system and Intel®(R) Core(TM) i3 CPU M330 @ 2.13GHz 4 GB RAM with Intel® HD Graphics card. Some parts of the simulations are done on an Oracle VM VirtualBox version 4.3.25, Linux operating system, Ubuntu 14.04.3 platform to run Virtual Gate vGate3.0 software[53]. Other imaging processing and analysis software also used on Windows machine, they are Scion Image ScnImage software[75], a Medical Imaging Data Examiner AMIDE[58], and OsiriX DICOM Viewer[76].

4.3 Experiments and Results

To perform our simulations, the patient model is built from digital phantom and his clinical MRI image. By following the algorithm illustrated in Figure 3.3,each patient model is injected with 11 independent different ^{18}F-FDG dosages calculated from equation(3.2). The scanner model is also built according to the technical specifications of real clinical scanner used for PET imaging system. After that, the PET imaging simulation is done for all patient models. Furthermore, according to the experiment scope, the patient models are divided into three different groups based on their age and weight. Finally, the resulting images and statistical values for those groups are used in system evaluation comparisons, image quality assessments and performance measurements. .

In this simulation, we choose brain as our main region of interest because it important region for PET imaging in clinical examination. In addition, the brain has frequent lesions and tumor occurrence beside other abnormality disease including Parkinson's disease and Alzheimer's disease.

4.3.1 Patient Model

As illustrated by Figure 3.2 presented in section 3.2.1, two digital volumes were used for developing our patient model: a real image from DICOM library and a digital anthropomorphic phantom based on Zubal phantom.

- **Real MRI Image**

We used BRANIX data set which is a set of DICOM files consisting of 1) *MRI images* data set associated with brain tumors. 2) *Data header*, called metadata that includes image information such as image type, modality, matrix dimensions, patient name, patient age and patient weight.

MATLAB is very useful tool in processing the DICOM image data as well as read its metadata. Figure 4.1 illustrate the result of reading a series of transverse MRI brain images from DICOM file. The metadata associated with this image is presented in Figure 4.2.

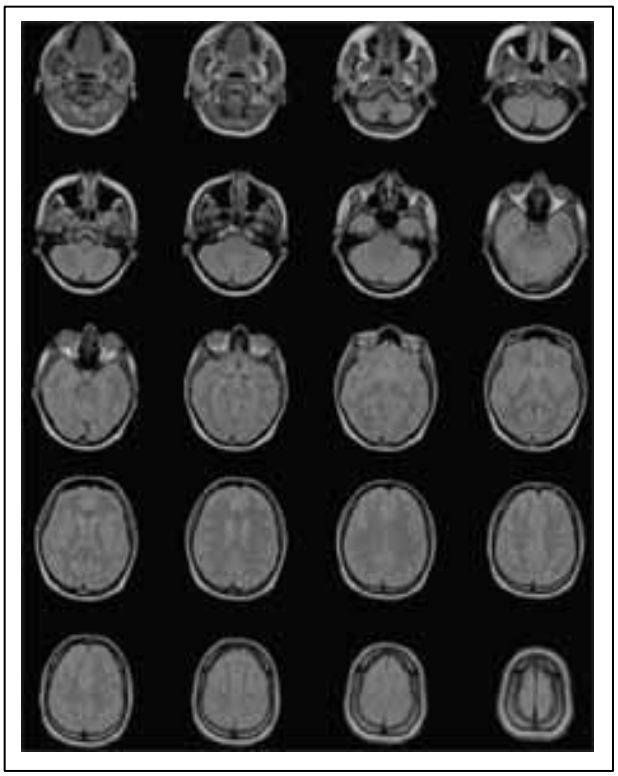

Figure 4.1 MRI brain image from DICOM library

```
                        Filename: 'brain_001.dcm'
                     FileModDate: '13-Apr-2001 11:57:59'
                        FileSize: 132914
                          Format: 'DICOM'
                   FormatVersion: 3
                           Width: 256
                          Height: 256
                        BitDepth: 16
                       ColorType: 'grayscale'
                  SelectedFrames: []
                      FileStruct: [1x1 struct]
                StartOfPixelData: 1830
          MetaElementGroupLength: 180
     FileMetaInformationVersion: [2x1 double]
        MediaStorageSOPClassUID: '1.2.840.10008.5.1.4.1.1.4'
      MediaStorageSOPInstanceUID:
'0.0.0.0.1.8811.2.1.20010414115754.22431'
               TransferSyntaxUID: '1.2.840.10008.1.2.1'
         ImplementationClassUID: '0.0.0.0'
       ImplementationVersionName: 'NOTSPECIFIED'
    SourceApplicationEntityTitle: 'NOTSPECIFIED'
                       ImageType: 'ORIGINAL\PRIMARY\MPR'
                     SOPClassUID: '1.2.840.10008.5.1.4.1.1.4'
                  SOPInstanceUID:
'0.0.0.0.1.8811.2.1.20010414115754.22431'
                       StudyDate: '20010316'
                      SeriesDate: '20010316'
                 AcquisitionDate: '20010316'
                       ImageDate: '20010323'
                       StudyTime: '143008'
                      SeriesTime: '143414'
                 AcquisitionTime: '143415'
                       ImageTime: '143006'
                 AccessionNumber: ''
                        Modality: 'MR'
                    Manufacturer: 'GE Medical Systems'
                InstitutionName: 'GENERAL HOSPITAL'
        ReferringPhysiciansName: [1x1 struct]
                    StationName: 'MRS1'
               StudyDescription: 'BRAIN'
             SeriesDescription: 'FSE PD AXIAL OBL'
       PerformingPhysiciansName: [1x1 struct]
                  OperatorsName: [1x1 struct]
         ManufacturersModelName: 'SIGNA'
                   PatientsName: [1x1 struct]
                      PatientID: '1235645'
             PatientsBirthDate: ''
                    PatientsSex: 'F'
                    PatientsAge: '028Y'
                 PatientsWeight: 61.2350
       AdditionalPatientHistory: ''
                ScanningSequence: 'SE'
                 SequenceVariant: 'SK'
                     ScanOptions: 'SP'
               MRAcquisitionType: '2D'
                    SequenceName: 'fse'
                 SliceThickness: 5
                 RepetitionTime: 2300
                        EchoTime: 22
                NumberOfAverages: 1
                ImagingFrequency: 63.8615
                     EchoNumbers: 1
           MagneticFieldStrength: 1.5000
            SpacingBetweenSlices: 2
     NumberOfPhaseEncodingSteps: 256
```

Figure 4.2 Metadata associated with MRI image presented in Figure 4.1

- **Zubal Phantom**

It is a set of a computerized head phantom. It is formed by a high resolution, well-segmented MRI image sequence of 35years old healthy male weighted 63 KG and measuring 155 cm in height. It is have been stored in three different datasets. In this simulation, we selected the second dataset which consists of 128 images each of them have a dimension of 256*256 pixel and 1.5 cm^3 voxel size. Each voxel is associated with a label corresponding to specific internal brain structure.

This simulation focuses on the anterior portion of the brain matter (cerebrum) which contains mostly gray and white matter. The phantom simulation process described in section 3.2.4 is applied on the selected anthropomorphic phantom. The algorithm eliminates all non-cerebrum organs and tissues such as the skull, hair, eyes,nose, or any other structures placed inside the human head. Then, the radiotracer distribution based on the patient data and radiotracer ratio (Figure 3.4) is set in order to form an emission map. By using the same procedure and Table 3.1, the attenuation map of this model is formed. An example of applying the above examination on image number 45 from Zubal phantom is shown in the following Figures.

Figure 4.3 illustrates the original selected MRI image from Zubal phantom before excluding the non-cerebral structures. Figure 4.4 presents the MRI image after exclusion. Figure 4.5 shows the resulting attenuation coefficient map. Figure 4.6 and Figure 4.7. present the resulting emission map of injected radiotracer activity amount equal to 370 MBq and 600 MBq, which are typical and maximum recommended radiotracer injection. All further PET imaging simulation processes and experiments will be performed on this constructed patient model.

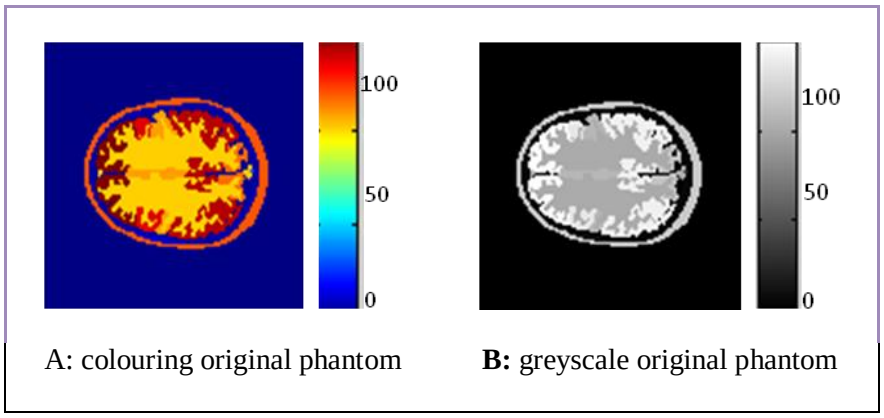

A: colouring original phantom **B:** greyscale original phantom

Figure 4.3 Original MRI phantom image for the proposed patient model

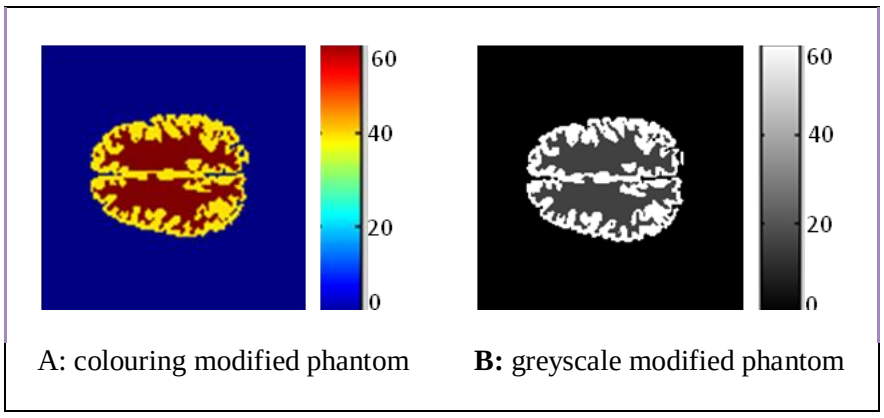

A: colouring modified phantom **B:** greyscale modified phantom

Figure 4.4 MRI phantom for the proposed Patient model after excluding non-cerebral structures

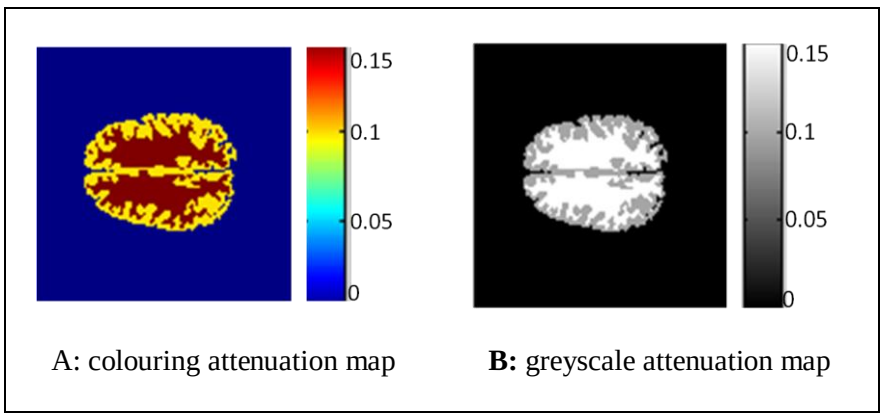

A: colouring attenuation map **B:** greyscale attenuation map

Figure 4.5 Attenuation coefficient map for the proposed patient model

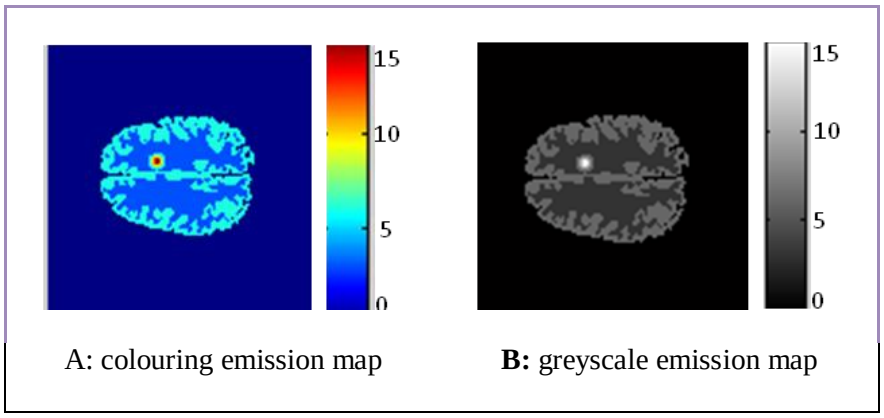

A: colouring emission map **B:** greyscale emission map

Figure 4.6 Emission map of the proposed patient model when the total injected radiotracer amount = 370MBq

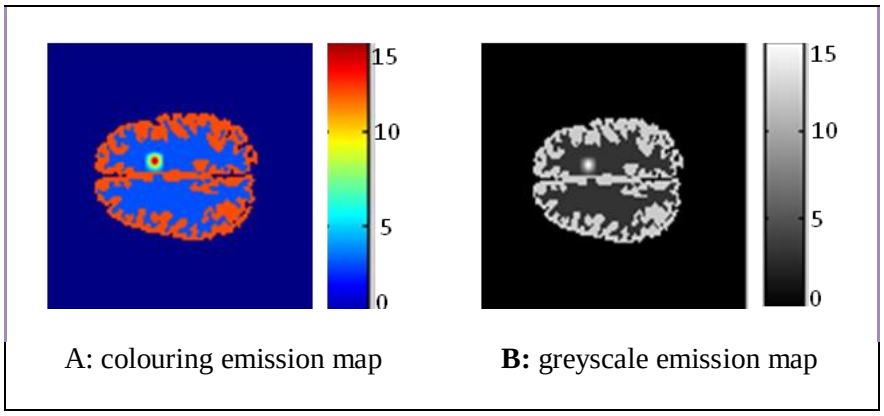

A: colouring emission map **B:** greyscale emission map

Figure 4.7 Emission map of the proposed patient model when the total injected radiotracer amount = 600MBq

4.3.2 Scanner Model

In the current simulations, a commercial clinical PET system, Siemens Biograph2 clinical PET scanner is modelled. This system model in GATE was extensively validated using clinical data as specify by NEMA and it's widely available in clinical daily routine. The Biograph2 PET scanner is a cylindrical type of scanner. The simulation parameters of the scanner are set as follows: detectors ring with radius 412.5 mm. Each detector is made of blocks crystal array. The dimension of each crystal element are 6.45*6.45*25 mm, axial field of view 180 mm, and scanning time is 60s. Table 4.1 summarizes the system geometry and scanning conditions

considered in the simulation processes. The real and simulated scanner is presented in Figure 4.8.

A: Biograph2 PET scanner

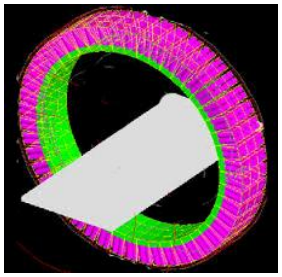

B: simulated Biograph2 PET

Figure 4.8 Physical and simulated illustration of the proposed scanner model

Table 4. 1 Specifications and features of the Siemens Biograph2 scanning system[12]

TECHNICHAL SPECIFICATION	
axial field of view, mm	180
Crystal Size, mm	6.5 x 6.5x25
Patient Weight Limit Kg	204
Power Supply Voltage	PET: 230 VAC, 50/60 Hz,
PROCESSOR SYSTEM	
Acquisition CPU	Syngo-based Windows platform
storage capacity	>100 GB HD
Image processor	Intel Pentium 4
storage capacity	>128 GB, 100,000 images (online)

The accuracy of the proposed scanner model was validated by comparing the obtained simulation results with the measured results obtained from physical real scanner according to performance measurement parameters recommended by NEMA performance protocols such as spatial resolution, sensitivity and scatter fraction. In

validation experiments ,The simulated results produce for each scanning session directly compared with the real experimental data obtained from[77], [78].

- **Spatial Resolution**

Spatial resolution is the ability of the simulated system to differentiate between two adjacent points in an image. It is measured in the simulated system by placing a patient phantom at a different position in the scanner from the scanner center in axial, trans-axial and radial direction (figure 4.9) by following the NEMA performance procedure. Table 4.2 contains the experiment results for the axial and radial direction for each phantom placed at 10 an 100 mm from the scanner center.

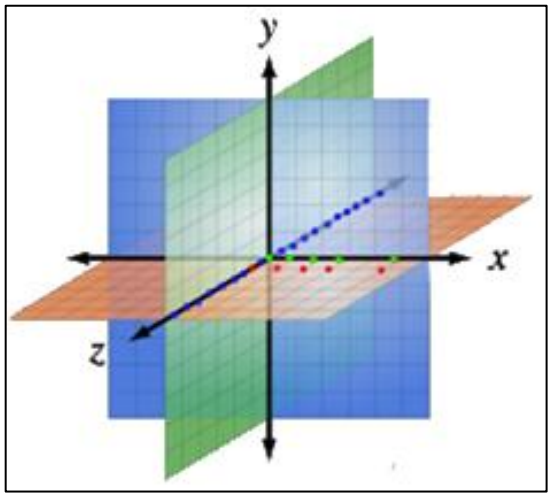

Figure 4.9 Direction at which spatial resolution measured. axial direction (blue), radial direction (green) and trans-axial direction (red)

Table 4.2 Spatial resolution for two different phantom positioned at 10 and 100 mm from the center of the proposed scanner model

	EXPERIMENTAL MEASUREMENTS		EXPERIMENTAL SIMULATIONS RESULTS	
Phantom position	10	100	10	100
Radial direction	6.12	7.02	5.43	6.54
Axial direction	6.25	6.65	5.56	5.93
Trans-axial direction	5.89	6.31	5.24	5.71

- **Sensitivity**

The sensitivity of the simulated scanner is defined as the scanner ability to detect the annihilation photons. In NEMA protocol, the sensitivity of the scanner is measured by counting the number of detected photon coincidence event per second (cps) for a given radiotracer amount expressed in MBq. Table 4.3 presents a comparison of the measured and simulated sensitivity of our scanner model when the phantom is placed at the 0 and 100 mm from the scanner center.

Table 4.3 Simulated and measured values of the sensitivity of our proposed scanner model

	EXPERIMENTAL MEASUREMENTS		EXPERIMENTAL SIMULATIONS RESULTS	
Phantom position	0 mm	100 mm	0 mm	100 mm
Sensitivity	6722 cpc/MBq	7237cpc/MBq	6785 cpc/MBq	7282 cpc/MBq
Ratio (0 mm/100 mm)	0.929		0.932	

- **Scatter Fraction**

In NEMA performance protocol, the scatter fraction in specific photon energy is the ratio of scattered coincidence events to the total number of coincidence events. For sufficiently low photon energy such as in our experiment, random coincidence is very small and can be discarded. Therefore, the measured total events are the sum of true and scatter events only. In Table 4.4 we illustrate the results of computing the scatter fraction of our scanner model in two intervals of photon energy {300,650}KeV and {425,650} KeV.

Table 4.4 Simulated and measured value of the scatter fraction experiment of our proposed scanner model

	EXPERIMENTAL MEASUREMENTS		EXPERIMENTAL SIMULATIONS RESULTS	
Photon Energy, keV	300-650	425-650	300-650	425-650
Scatter Fraction	45.3%	34.1%	44.1%	33.4%

4.3.3 Simulated PET Image Quality Assessment

With the goal of assessing the relationship between the quality of simulated PET image, the amount of radiotracer injected to the patient and the patient's physical parameters (age, weight), we investigate a set of simulation studies based on the image quality measurement introduced in section 3.6.3. For those studies, we have performed PET imaging simulations with the PET scanner model and the patient model proposed earlier. We simulated a set of 60 patients provided in the DICOM data set with the range of weight from 40 to 150 Kg, and adult ages distribution from 20 to 95. From the given weight range and for constant age, we can divide the patients dataset into three groups: slim patients (group of patients with very low weight,45≥weight) , medium-weight patients (group of patients with moderate weight, 45<weight<70), obese patients (group of patient with a heavy weight,70≤weight<90) and overweight patients (group of patient with weight ≥90).

The range of the injected radiotracer in the simulation was chosen to cover the radiotracer amount given to the patients in PET centres based on our proposed initial injection radioactive A calculation equation introduced in section 3.2.3.

$$A = \left[\frac{patient\ age\ (year)}{patient\ age(year) + 12}\right] * 7.2 * patient\ weight/min \pm 5 \qquad (4.1)$$

Also, in this study for each patient, we performed 11 independent PET imaging simulation with activity systematically covering the entire interval of recommended

amount radioactivity. Then, the NEC, SNR and lesion detectability (precision and recall) was computed for every simulation. The experimental results are classified as flowing:

- Computing the NEC, SNR for our default patient parameters weight=63 kg and age 35 years. This patient parameter is directly typical to the anthropomorphic phantom parameters. These results are illustrated on Table 4.5.

Table 4.5 Statistical parameters SNR and NEC for default scanner and patient model

Total injected Activity(MBq)	SNR(dB)	NEC(cps)
304	59.0221	3.4836e+03
321	59.1599	3.4999e+03
338	59.4232	3.5311e+03
355	59.6715	3.5607e+03
372	59.7905	3.5749e+03

- Calculating the optimal radiotracer injection amount for our default patient parameters in term of lesion and tumor detection. Table 4.6 provides the precision and recall values computing in this simulation.

Table 4.6 Lesion detection (precision and recall) for default patient model

Total injected Activity(MBq)	Precision	Recall
253	0.1364	0.1714
270	0.1705	0.2143
287	0.1818	0.2286
304	0.2727	0.3429
321	0.4545	0.5714
338	0.5455	0.6857
355	0.7955	1
372	0.8750	1
389	1	1
406	1	1
423	1	1

- Calculating the optimal radiotracer injection amount for patients with different weight in Kg, and constant age in year in term of lesion and tumor detection. Table 4.7 compares the recommendation, theoretical and experimental amount of injection radiotracer for randomly selected patients. The recommendation amount is the dose recommended by EANM dosage card[13], [14] .The theoretical dosage is the dose directly resulted from equation (4.1) and the experimental dose is the minimum injection dose with recall=1.

Table 4.7 Total injected activity for patients with different weight in Kg and fixed age in year, age=35 years

Weight (kg)	Recommended activity (MBq)	Theoretical activity (MBq)	Experimental activity (MBq)
40	300	215	313
55	346	295	339
63	370	338	355
70	454	375	375
90	504	383	383
113	600	605	435
120	600	643	510

- Calculating the optimal radiotracer injection amount for patients with fixed weight in Kg and different ages in term of lesion and tumor detection. As in above table, Table 4.8 shows examples of recommendation, theoretical, and experimental amount of injection radiotracer for randomly selected patients.

Table 4.8 Total injected activity for patients with fixed weight in Kg and diffrent age in year, weight=63 Kg

Age (year)	Recommended activity (MBq)	Theoretical activity (MBq)	Experimental activity (MBq)
20	370	284	355
35	370	338	355
48	370	363	358
55	370	372	360
63	370	381	362
70	370	382	362
90	370	400	362

Figure 4.10 and 4.11 show the details of how lesion detection process was computed when recall=1.Finally,in Figure 4.11 we show an example of image-based lesion detection experiments for patient with 63Kg and 70 years old and Table 4.9 illustrates the total injected radiotracer doses and their corresponding precision and recall values of the same simulation.

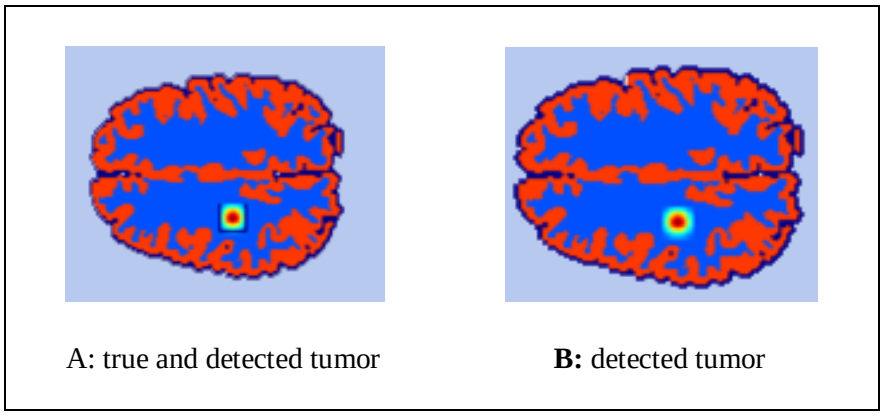

A: true and detected tumor **B:** detected tumor

Figure 4.10 True and detected tumours when recall=1

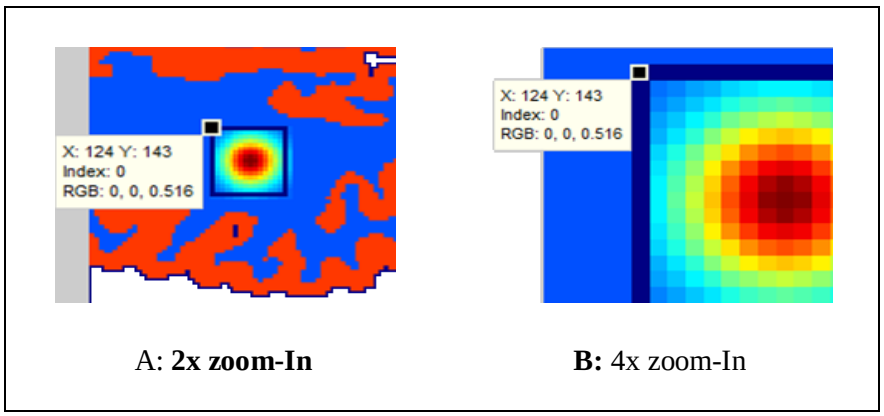

A: **2x zoom-In** **B:** 4x zoom-In

Figure 4.11 True and detected tumor when recall=1 (detailed view)

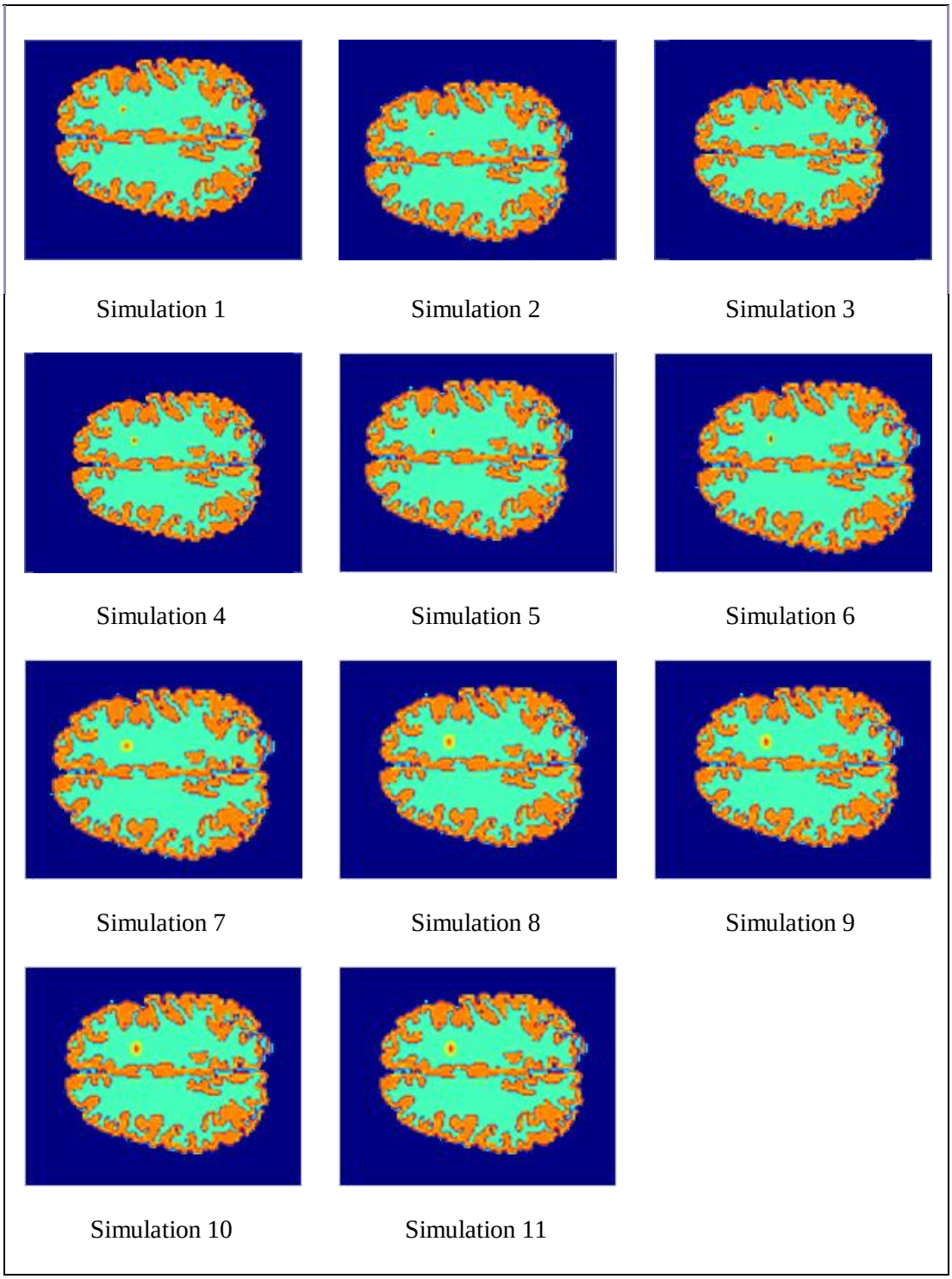

Figure 4.12 Image-based lesion detection experiments of 11 independent simulations for patient with 63Kg and 70 years

Table 4.9 Precision and recall values image-based lesion detection experiments of 11 independent simulations for patient with 63Kg and 70 years

Simulation	Total injected Activity(MBq)	Precision	Recall
1	247	0.1364	0.1714
2	267	0.1705	0.2143
3	286	0.1918	0.2286
4	305	0.3287	0.3429
5	324	0.4545	0. 6429
6	343	0.5455	0.9000
7	362	0.6443	1
8	382	0.8750	1
9	389	0. 9625	1
10	406	1	1
11	423	1	1

5 DISCUSSIONS

CHAPTER V

DISCUSSIONS

5.1 Introduction

This chapter reviews and discusses the main results obtained from the simulations performed in this thesis. For clarity, the discussion chapter is organized into sections corresponding to each of simulations illustrated in the previous chapter.

5.2 Patient Model

As shown in chapter 4, the PET imaging processes are simulated for 60 patients real MRI images. For each patient, we present our development of computational patient model used in the simulation. The model generated from the segmentation of patients' MRI image taken from BRAINX dataset and the digital anthropomorphic phantom Zubal phantoms were used in nuclear imaging researches. The phantom model produced a digital comparable data of the patients' image that corresponds to that obtained from the real clinical data with the PET imaging system. The patient model developed from segmented MRI image is of patient having 63Kg, 35 years and with a brain tumor is presented in section 4.3.1, Figures 4.3 - 4.7.

As in literature[3], [10], [12], [15], we conclude that the investigation of the computational patient model from real data is a fixable and efficient procedure to describe the physiology and anatomical structure of the patient body region under

study. In addition, the investigated patient model has a huge potential for predicting the optimal radiotracer injection dosage used in detecting abnormal lesions and tumors in a safe and reliable manner.

5.3 Scanner Model

In chapter 4, we presented the specifications followed to enable simulation of PET imaging systems in MATLAB platform and to deal with the data output from the simulated process. In order to reach equilibrium between simulated and real system output, the implemented class is validated according to the technical standards provided by the Association of Electrical Equipment and Medical Imaging Manufacturers NEMA. In this manner, we can use our simulation software results in the clinical practice to reconstruct the required examination data. Furthermore, due to its wide area of use in clinical application, SIEMENS Biograph 2 PET system was used in this work. Also, as stated in chapter 4, the evaluation parameter tested with our proposed model are: spatial resolution, sensitivity and scatter fraction. These parameters are directly compared with their respective values from real experimental data.

Figures 5.1 and 5.2 show the spatial resolution values obtained from the simulated scanner that are within 9% of the values obtained from the real scanner. We can conclude that the results of our simulation provide a performance improvement in term of the special resolution in comparison to the respective real measurements. These improvements are achieved by introducing an analytical distribution function for the positron emission and annihilation with a specific range 2.3mm. For the same factor, the analysis of the comparison between the simulated and real values of sensitivity evaluation metric shows that the simulated values provide improvement sensitivity (up to 2%) compared with the experimental sensitivity values. The

analysis comparisons are illustrated in Figure 5.3.Now, the evaluation comparison between simulated and real scatter fraction metric showed in Figure 5.4 indicates that in all cases the real scanner provides 2% to 3% had better scatter fraction values. The main aspect that causes this underestimation of the simulated model is the approximation of the scanner geometry used for our simulation model.

From the above evaluation results, we can conclude that the scanner model described in this study is validated,and the inconsistencies between the simulated and real data are tolerable. Consequently, this validated model can be used for PET optimization studies and their results can be directly implemented in clinical examination.

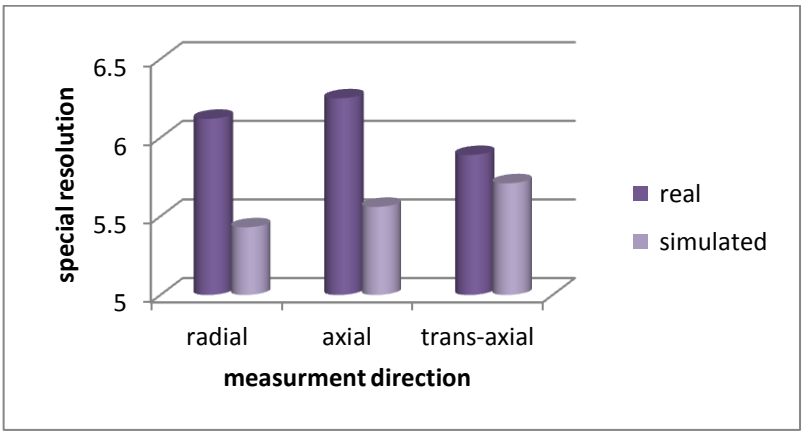

Figure 5.1 Spatial resolution for phantom positioned at 10 mm from the center of scanner ring

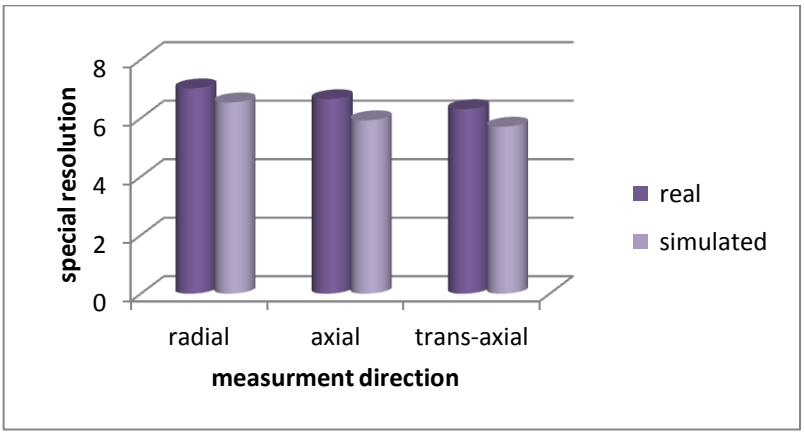

Figure 5.2 Spatial resolution for phantom positioned at 100 mm from the center of scanner ring

.

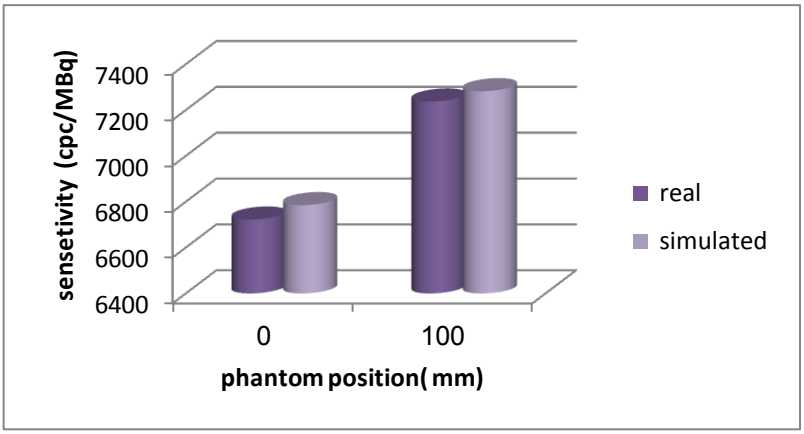

Figure 5.3 Sensitivity values for phantoms positioned at 0 and 100 mm from the center of scanner ring

.

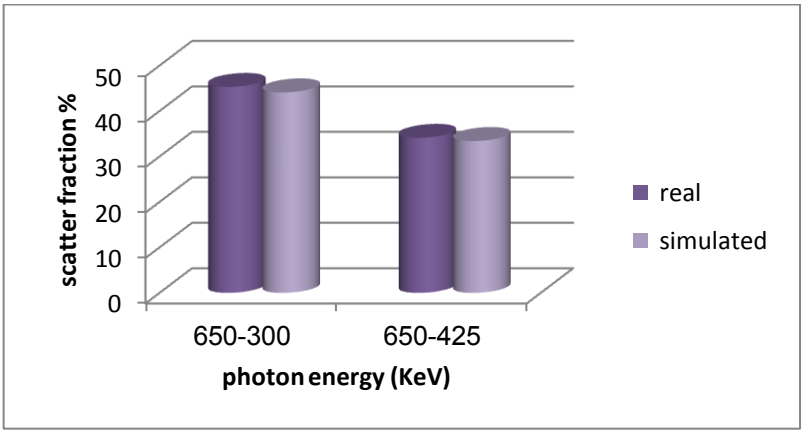

Figure 5.4 Scatter fraction evaluation measurement for two energy windows

5.4 Simulated PET Image Quality Assessment

The main goal of this thesis is to predict the minimal amount of injected radiotracer to the patient in order to achieve precise tumor detectability, sufficient image quality, and to reduce patient's radiation risk. To reach that goal, we performed a set of simulation studies based on the patient's physical parameters (age, weight)and fixed scanning time as described in sections 3.6.3 and 4.3.3.The simulation results are discussed according to the following categories:

- **Patient weighted 63 Kg and was 35 years old**

Figure 5.5 shows the NEC values associated with a moderate radiotracer amount injected to our default patient model. According to Figure 5.5 we can conclude that as the injected amount of radiotracer increases, the quality of the constructed sinogram ,the reconstructed PET image and the NEC values are increased. After the peak of NEC values is reached, as the injected amount of radiotracer increases, the NEC values are remaining the same and the quality of the constructed sinogram and the reconstructed PET image will stagnate as well.

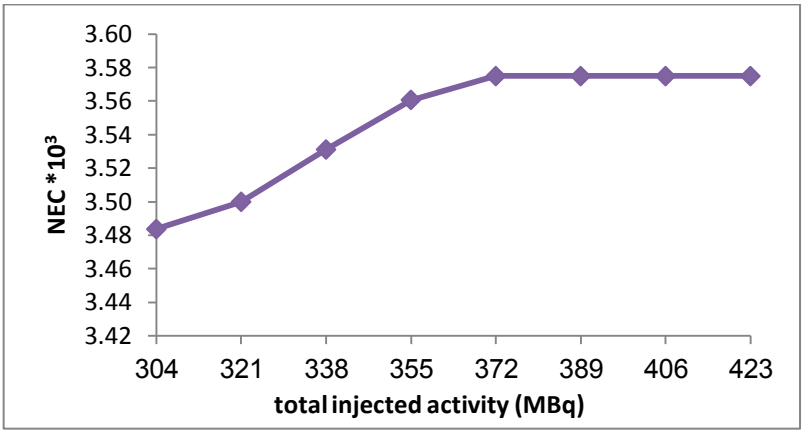

Figure 5.5 NEC values for default scanner and patient model

For the same patient, Figure 5.6 illustrates the evaluation results of calculating the optimal radiotracer injection amount in term of lesion and tumor detection based on precision and recall values. The optimal radiotracer amount according to our simulation is 355MBq that is 5% optimized compared to the clinical injection dosage which equals to 370MBq.Also, it discrepancy from the calculated initial dosage value 338 MBq by 5%.

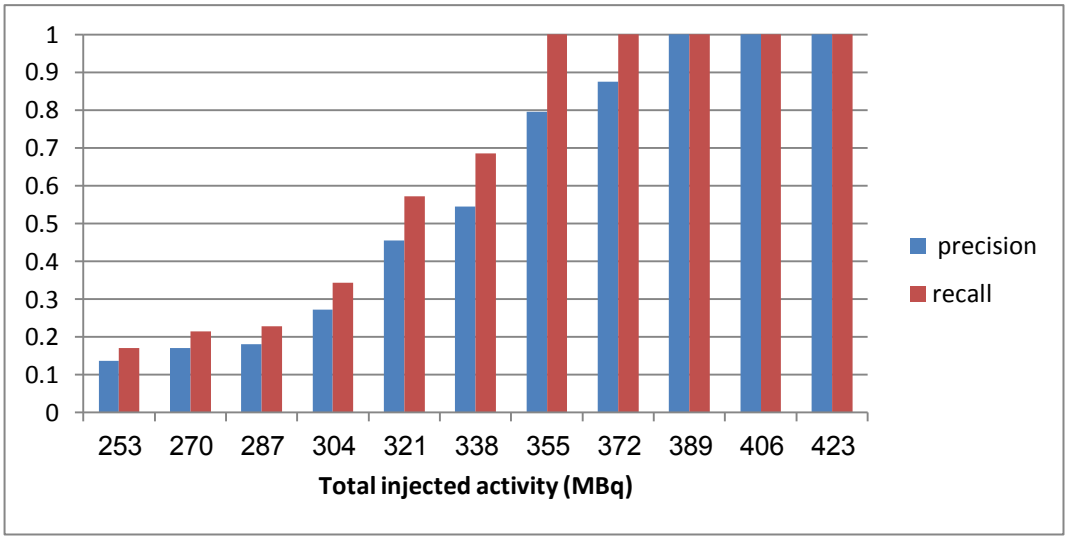

Figure 5.6 Lesion detection (precision and recall) for default patient model

- **Patients with different weight and constant age**

Figure 5.7 illustrates the evaluation results of calculating the optimal radiotracer injection amount in terms of lesion and tumor detection based on precision and recall values for a set of randomly selected patients from the available dataset of 60 patients.

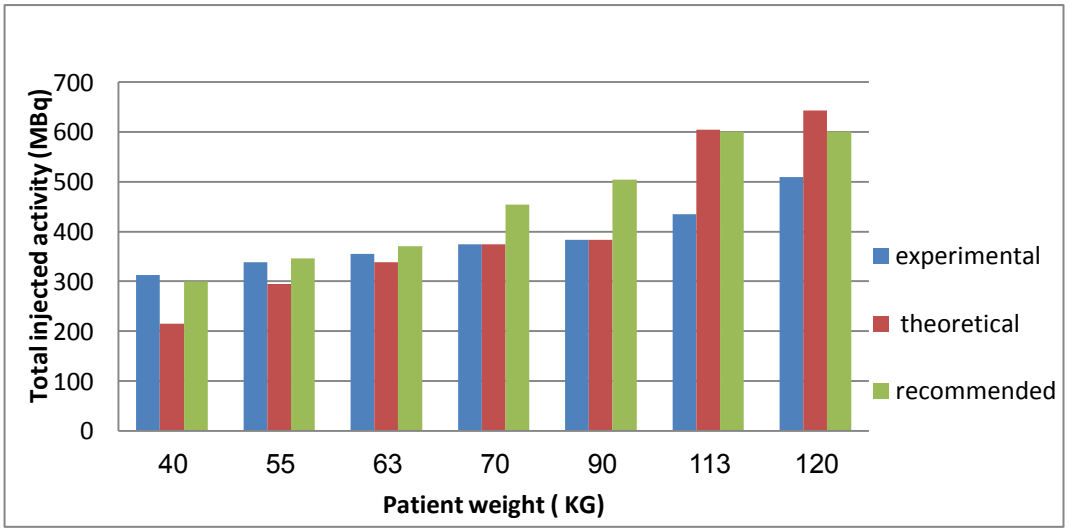

Figure 5.7 Total injected activity for patients with different weight (Kg) and fixed age (=35 years)

Comparisons of the simulator, recommended and theoretical calculating injected dosage according to the patients groups divided in section 4.3.3and illustrated in Figure 5.8 are:

- For the group of slim patients, the minimal injected radiotracer amount that provides accurate lesion detection by the simulator is 4% greater than the clinical recommendation dosage and up to 45% greater than the initial theoretical calculating dosage.
- For the group of medium weight patients, the simulator dosage is optimizing the clinical recommendation dosage approximately by 5% to 7% and they are greater than the initial computed dosage by approximately 5%.
- For the group of obese patients, the simulator and the initial theoretical dosage are equal and they are optimizing the clinical recommendation dosage by 17% to 24%.
- For the group of overweight patients, the simulator dosage is optimizing the clinical recommendation dose and the initial theoretical dose by values up to 28%.

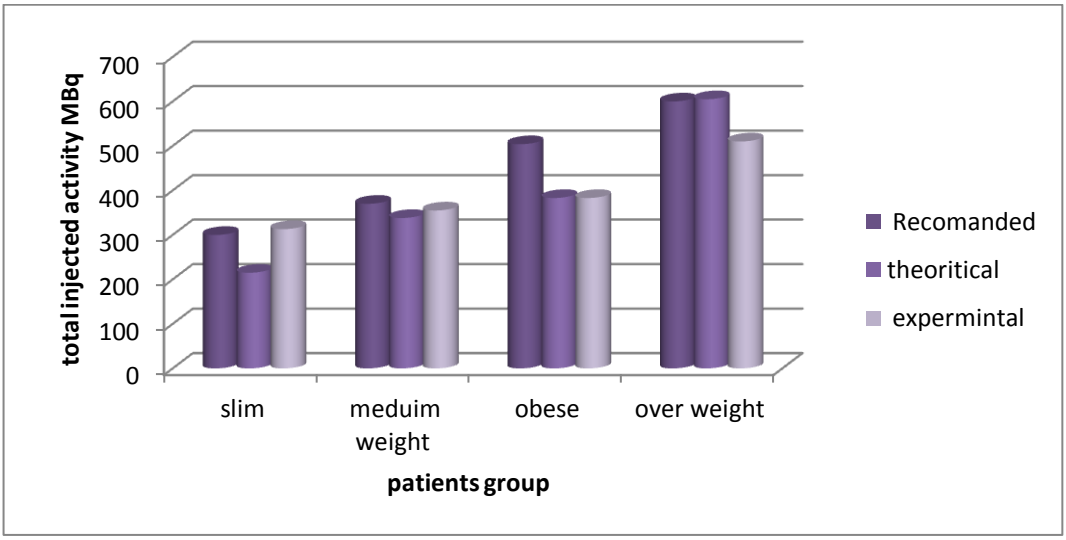

Figure 5. 8 Total injected activity for different patients groups

- **patients with fix weight (Kg)and different ages (years)**

Figure 5.9 illustrates the evaluation results of calculating the optimal radiotracer injection amount in terms of lesion and tumor detection based on precision and recall values for a set of randomly selected patients. The comparative evaluation between simulator, clinical recommendation and the theoretically calculated dosage shows a discrepancy values for the theoretical dosage among patients. Also, the simulator dosage provides 4% to 5% optimization to the clinicaly recommended dosage of injected radioactive substance.

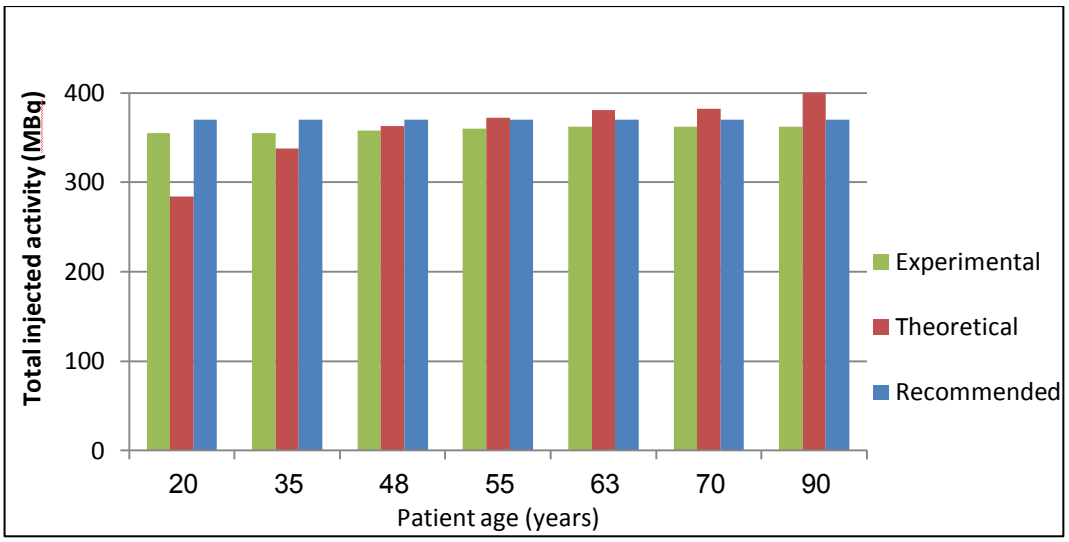

Figure 5.9 Total injected activity for patients with fixed weight (Kg) and different age (years) weight=63 Kg

From the above results, we can conclude that our simulator can perform a desirable and efficient prediction of injection radiotracer amount that optimizes the current clinical amount up to 28%. In addition, we can conclude that the total injected radiotracer dosage for adult patients are mostly affected when considering patient weight rather than patient age.

5.5 Execution Time

All the simulations in this study are monitored (in seconds) to assess the time consumed to execute certain simulation processes. Figure 5.10 illustrates the execution log file for lesion detecting simulation for patient with 63Kg and age 70 years old. This log file shows that the total execution time is 1712 s which is equal to 20 min as estimated by [57]

Function Name	Calls	**Total Time**	Self Time*	Total Time Plot (dark band = self time)
simulatePETv1	1	1711.714 s	8.288 s	
PETrec	11	833.059 s	831.835 s	
fusion	11	697.608 s	0.744 s	
nlfilter	66	695.669 s	65.484 s	
fusion>@(x)std2(x(:))	4322835	533.568 s	65.743 s	
std2	4322835	467.825 s	70.017 s	
std	4322835	397.809 s	68.149 s	
var	4322835	329.660 s	329.660 s	
PETprocess	11	167.259 s	167.257 s	

Figure 5.10 PET simulation execution time profile

6 CONCLUSION & FUTURE WORK

CHAPTER VI

CONCLUSION & FUTURE WORK

6.1 Conclusion

In this thesis, a PET imaging simulation tool for physical and clinical research was proposed. This simulator can be easy to learn and use by beginners, temporary users (patients), researchers and it does not require a programming and a PET scanning background. Compared to other simulation platforms, our proposing tool can be operated on common PCs and has a good trade-off between performance and the computational resources used. This tool efficiently reconstructs a PET image both from digital anthropomorphic phantom and real patient image. The simulation includes pre-processing of the patient image, calculating the radiotracer injection dosage, positron range distribution, PET image reconstruction and PET image quality measurements.

The main purpose of this study is to predict the optimal radiotracer injected dosage for adult patients. To achieve our goal, we performed a set of simulations to assessing the relationship between the quality of simulated PET image, the amount of radiotracer injected to the patient and the patient's physical parameters (age, weight). Each simulation is done using the PET scanner model and the patient model to

diagnostic task (tumor/lesion detection), it calculates the PET image quality assessment variables NEC and SNR. From the results of those simulations, we conclude that our simulator can drive a desirable and efficient prediction of injection radiotracer amount that optimizes the current clinical amount up to 28%. In addition, we can conclude that the total injected radiotracer dosage for adult patients are mostly affected by the patient weight rather than by the patient age.

The proposed PET system was evaluated according to National Electrical Manufacturers Association (NEMA) requirements in order to apply our simulation results into the clinical applications. We notice that our proposed system provides a 9% improvement to the real PET system. Furthermore, our proposed system passes the NEMA validation test and it is qualified to use directly in PET optimization studies.

6.2 Limitation

We observe that our simulator does not provide accurate results with the very small input values of the scanner parameters: crystal size and scanner ring radius. In addition, in this simulation, we assumed no attenuation correction and assumed fixed value of positron range and annihilation.

In addition, the dosage optimization study is focused only on an adult patient because EANM provides a specific dosage card for children that minimize the effective radiation dose among patients beside the selected digital anthropomorphic phantom support.

6.3 Future Work

In order to build more realistic model of PET scanner systems and to be able to test more sophisticated situation, this work can be improvement in several ways:

- Adding additional system data, for example, dead time of the detector, radioactive decay, full width at half-maximum, time-of-flight information.
- Improving the system sensitivity and accuracy by exploring more efficient methods such as parallax error reducing algorithm.
- Introducing more efficient random number generators in order to enhance the resulting statistical value.
- Increasing the accuracy of the predicted injection dosage by introducing one of the time dependent processes involved in PET scanning such as radiotracer alternation over time passage, the scanner motion during the acquisition process and the patient breathing while scanning.
- Expand the dosage optimization study to include children and old patient in additions to adult patients.

LIST OF REFERENCES

[1] O. Mawlawi and D. W. Townsend, "Multimodality imaging: an update on PET/CT technology," *Eur. J. Nucl. Med. Mol. Imaging*, vol. 36, no. 1, pp. 15–29, 2009.

[2] S. R. Cherry, "Multimodality imaging: Beyond pet/ct and spect/ct," in *Seminars in nuclear medicine*, 2009, vol. 39, pp. 348–353.

[3] S. E. de O. B. Silva, "Small animal PET imaging using GATE Monte Carlo simulations: Implementation of physiological and metabolic information," 2010.

[4] J. E. Gillam and M. Rafecas, "Monte-Carlo simulations and image reconstruction for novel imaging scenarios in emission tomography," *Nucl. Instrum. Methods Phys. Res. Sect. Accel. Spectrometers Detect. Assoc. Equip.*, vol. 809, pp. 76–88, 2016.

[5] A. Turco, "Monte Carlo simulations of a small-animal PET scanner. Analysis of performances and comparison between camera designs," 2012.

[6] H. Zaidi, "Relevance of accurate Monte Carlo modeling in nuclear medical imaging," *Med. Phys.*, vol. 26, no. 4, pp. 574–608, 1999.

[7] M. Ljungberg, "Simulation Techniques and Phantoms," in *Emission Tomography , The Fundamentals of PET and SPECT*, Elsevier Inc., 2004, pp. 551–563.

[8] H. Zaidi and G. Sgouros, *Therapeutic applications of Monte Carlo calculations in nuclear medicine*. CRC Press, 2002.

[9] H. Zaidi and K. Koral, "Scatter Correction Strategies in Emission Tomography," in *Quantitative Analysis in Nuclear Medicine Imaging*, Springer Science, 2006, pp. 205 – 235.

[10] J. Boldyš, J. Dvořák, M. Skopalová, and O. Bělohlávek, "Monte Carlo simulation of PET images for injection dose optimization," *Int. J. Numer. Methods Biomed. Eng.*, vol. 29, no. 9, pp. 988–999, 2013.

[11] S. R. Cherry, J. A. Sorenson, and M. E. Phelps, *Physics in nuclear medicine*. Elsevier Health Sciences, 2012.

[12] N. A. Karakatsanis, G. Loudos, A. Rahmim, and K. S. Nikita, "Monte-Carlo based characterization of the counting rate (NECR) response for personalized optimization of the administered activity in clinical PET imaging," *Front. Biomed. Technol.*, vol. 1, no. 1, pp. 14–34, 2014.

[13] R. Boellaard, M. J. O'Doherty, W. A. Weber, F. M. Mottaghy, M. N. Lonsdale, S. G. Stroobants, W. J. Oyen, J. Kotzerke, O. S. Hoekstra, and J. Pruim, "FDG PET and PET/CT: EANM procedure guidelines for tumour PET imaging: version 1.0," *Eur. J. Nucl. Med. Mol. Imaging*, vol. 37, no. 1, pp. 181–200, 2010.

[14] A. Varrone, S. Asenbaum, T. Vander Borght, J. Booij, F. Nobili, K. Någren, J. Darcourt, Ö. L. Kapucu, K. Tatsch, and P. Bartenstein, "EANM procedure guidelines for PET brain imaging using [18F] FDG, version 2," *Eur. J. Nucl. Med. Mol. Imaging*, vol. 36, no. 12, pp. 2103–2110, 2009.

[15] J. Dvořák, J. Boldyš, M. Skopalová, and O. Bělohlávek, "Application of the random field theory in PET imaging-injection dose optimization," *Kybernetika*, vol. 49, no. 2, pp. 280–300, 2013.

[16] T. Saga, "Molecular imaging of cancer with positron emission tomography," *Jpn. J. Clin. Radiol.*, vol. 56, no. 3, pp. 311–319, 2011.

[17] S. A. Kane, *Introduction to physics in modern medicine*. Taylor & Francis, 2009.

[18] K. M. Waterstram-Rich and P. E. Christian, *Nuclear medicine and PET/CT: technology and techniques*. Elsevier Health Sciences, 2013.

[19] Brian F Hutton, "overview of iterative reconstruction applied to PET (and SPECT)," Institute of Nuclear Medicine University College London.

[20] P. E. Valk, *Positron emission tomography: basic sciences*. Springer Science & Business Media, 2003.

[21] S. R. Cherry and M. Dahlbom, "PET: physics, instrumentation, and scanners," in *PET*, 2006, pp. 1–117.

[22] I. Verel, G. W. Visser, and G. A. van Dongen, "The promise of immuno-PET in radioimmunotherapy," *J. Nucl. Med.*, vol. 46, no. 1 suppl, p. 164S–171S, 2005.
[23] C. L. Melcher, "Scintillation crystals for PET," *J. Nucl. Med.*, vol. 41, no. 6, p. 1051, 2000.

[24] M. N. Wernick and J. N. Aarsvold, *Emission tomography: the fundamentals of PET and SPECT*. Academic Press, 2004.

[25] P. Zanzonico, "Principles of nuclear medicine imaging: planar, SPECT, PET, multi-modality, and autoradiography systems," *Radiat. Res.*, vol. 177, no. 4, pp. 349–364, 2012.

[26] J. L. Humm, A. Rosenfeld, and A. Del Guerra, "From PET detectors to PET scanners," *Eur. J. Nucl. Med. Mol. Imaging*, vol. 30, no. 11, pp. 1574–1597, 2003.

[27] T. K. Lewellen, "The challenge of detector designs for PET," *Am. J. Roentgenol.*, vol. 195, no. 2, pp. 301–309, 2010.

[28] M. Jacobson, R. Levkovitz, A. Ben-Tal, K. Thielemans, T. Spinks, D. Belluzzo, E. Pagani, V. Bettinardi, M. C. Gilardi, and A. Zverovich, "Enhanced 3D PET OSEM reconstruction using inter-update Metz filtering," *Phys. Med. Biol.*, vol. 45, no. 8, p. 2417, 2000.

[29] R. M. Lewitt and S. Matej, "Overview of methods for image reconstruction from projections in emission computed tomography," *Proc. IEEE*, vol. 91, no. 10, pp. 1588–1611, 2003.

[30] D. L. Bailey, "Quantitative procedures in 3D PET," in *The theory and practice of 3D PET*, Springer, 1998, pp. 55–109.
[31] B. Bendriem and D. W. Townsend, *The theory and practice of 3D PET*, vol. 32. Springer Science & Business Media, 2013.

[32] A. C. Kak and M. Slaney, *Principles of computerized tomographic imaging*. Society for Industrial and Applied Mathematics, 2001.

[33] B. F. Hutton, M. Braun, and P. Slomka, *Image registration techniques in nuclear medicine imaging*. Springer, 2006.

[34] G. B. Saha, *Basics of PET imaging: physics, chemistry, and regulations*. Springer Science & Business Media, 2010.

[35] E. E. Kim, "Clinical PET-CT in Radiology: Integrated Imaging in Oncology," *J. Nucl. Med.*, vol. 53, no. 3, pp. 505–505, 2012.

[36] M. Beister, D. Kolditz, and W. A. Kalender, “Iterative reconstruction methods in X-ray CT,” *Phys. Med.*, vol. 28, no. 2, pp. 94–108, 2012.

[37] P. P. Bruyant, “Analytic and iterative reconstruction algorithms in SPECT,” *J. Nucl. Med.*, vol. 43, no. 10, pp. 1343–1358, 2002.

[38] V. Kapoor, B. M. McCook, and F. S. Torok, “An Introduction to PET-CT Imaging 1,” *Radiographics*, vol. 24, no. 2, pp. 523–543, 2004.

[39] H. Zaidi and X. G. Xu, “Computational anthropomorphic models of the human anatomy: the path to realistic Monte Carlo modeling in radiological sciences,” *Annu Rev Biomed Eng*, vol. 9, pp. 471–500, 2007.

[40] J. Peter, M. Tornia, and R. Jaszczek, “Analytical versus voxelized phantom representation for Monte Carlo simulation in radiological imaging.,” *Medical Imaging, IEEE Transactions on*, vol. 19, no. 5, pp. 556 – 564, 2000.

[41] M. Ljungberg, S.-E. Strand, and M. A. King, *Monte Carlo calculations in nuclear medicine: Applications in diagnostic imaging*. CRC Press, 2012.

[42] I. G. Zubal, C. R. Harrell, E. O. Smith, Z. Rattner, G. Gindi, and P. B. Hoffer, “Computerized three-dimensional segmented human anatomy,” *Med. Phys.*, vol. 21, no. 2, pp. 299–302, 1994.

[43] W. P. Segars, G. Sturgeon, S. Mendonca, J. Grimes, and B. M. Tsui, “4D XCAT phantom for multimodality imaging research,” *Med. Phys.*, vol. 37, no. 9, pp. 4902–4915, 2010.

[44] I. Buvat and I. Castiglioni, “Monte Carlo simulations in SPET and PET,” *Q. J. Nucl. Med. Mol. Imaging*, vol. 46, no. 1, p. 48, 2002.

[45] P. Andreo, “Monte Carlo techniques in medical radiation physics,” *Phys. Med. Biol.*, vol. 36, no. 7, p. 861, 1991.

[46] I. G. Zubal and C. R. Harrell, “Voxel based Monte Carlo calculations of nuclear medicine images and applied variance reduction techniques,” *Image Vis. Comput.*, vol. 10, no. 6, pp. 342–348, 1992.

[47] F. Salvat, J. M. Fernández-Varea, J. Sempau, and J. Mazurier, “Practical aspects of Monte Carlo simulation of charged particle transport: mixed algorithms and variance reduction techniques,” Radiat. Environ. Biophys., vol. 38, no. 1, pp. 15–22, 1999.

[48] A F Biela jew, H Hirayama and , W R Nelsony and D W O Rogers, *the Electron Gamma Shower (EGS)*.

[49] Los Alamos National Laboratory, *A General Monte Carlo N-Particle (MCNP) Transport Code*.

[50] S. Agostinelli, J. Allison, K. al Amako, J. Apostolakis, H. Araujo, P. Arce, M. Asai, D. Axen, S. Banerjee, and G. Barrand, "Geant4—a simulation toolkit," *Nucl. Instrum. Methods Phys. Res. Sect. Accel. Spectrometers Detect. Assoc. Equip.*, vol. 506, no. 3, pp. 250–303, 2003.

[51] Francesc Salvat, *PENELOPE2014, A Code System for Monte-Carlo Simulation of Electron and Photon Transport*. 2014.

[52] *simSET:Simulation System for Emission Tomography*. The University of Washington Imaging Research Laboratory, 2014.

[53] OpenGATE collaboration, *GATE,imulations of Preclinical and Clinical Scans in Emission Tomography, Transmission Tomography and Radiation Therapy*. .

[54] Irène Buvat, "Simulations in emission tomography using GATE," presented at the Laboratory of Functional Imaging, U678 INSERM, Paris, France, 2007.

[55] R. L. Harrison, "Simulation of medical imaging systems: emission and transmission tomography," in *Handbook of Particle Detection and Imaging*, Springer, 2012, pp. 1095–1124.

[56] C. Lee, *Monte Carlo Calculations in Nuclear Medicine Second Edition: Applications in Diagnostic Imaging*. LWW, 2014.

[57] S. Yu, "Simulation of PET Brain Images Using Monte Carlo Method," Master Thesis in Medical Imaging, School of Technology and Health Royal Institute of Technology, Stockholm, Sweden, 2010.

[58] *AMIDE: Amide's a Medical Imaging Data Examiner*. GNU General Public License version 2.0 (GPLv2).

[59] A. Piepsz, K. Hahn, I. Roca, G. Ciofetta, G. Toth, I. Gordon, J. Kolinska, and J. Gwidlet, "A radiopharmaceuticals schedule for imaging in paediatrics," *Eur. J. Nucl. Med.*, vol. 17, no. 3–4, pp. 127–129, 1990.

[60] S. T. Treves, A. Baker, F. H. Fahey, X. Cao, R. T. Davis, L. A. Drubach, F. D. Grant, and K. Zukotynski, "Nuclear medicine in the first year of life," *J. Nucl. Med.*, vol. 52, no. 6, pp. 905–925, 2011.

[61] R. Accorsi, J. S. Karp, and S. Surti, "Improved dose regimen in pediatric PET," *J. Nucl. Med.*, vol. 51, no. 2, pp. 293–300, 2010.

[62] J. Cal-González, J. L. Herraiz, S. España, M. Desco, J. J. Vaquero, and J. M. Udías, "Positron range effects in high resolution 3D PET imaging," in *Nuclear Science Symposium Conference Record (NSS/MIC), 2009 IEEE*, 2009, pp. 2788–2791.

[63] Robley Evans, in *The Atomic Nucleus*, New York: McGraw-Hill, 1972, p. 628.

[64] C. S. Levin and E. J. Hoffman, "Calculation of positron range and its effect on the fundamental limit of positron emission tomography system spatial resolution," *Phys. Med. Biol.*, vol. 44, no. 3, p. 781, 1999.

[65] C. J. Thompson, J. Moreno-Cantu, and Y. Picard, "PETSIM: Monte Carlo simulation of all sensitivity and resolution parameters of cylindrical positron imaging systems," *Phys. Med. Biol.*, vol. 37, no. 3, p. 731, 1992.

[66] G. Steinbrecher and W. T. Shaw, "Quantile mechanics," *Eur. J. Appl. Math.*, vol. 19, no. 02, pp. 87–112, 2008.

[67] W. Gilchrist, *Statistical modelling with quantile functions*. CRC Press, 2000.

[68] L. A. Grzelak, J. Witteveen, M. Suarez-Taboada, and C. W. Oosterlee, "The Stochastic Collocation Monte Carlo Sampler: Highly Efficient Sampling from'Expensive'Distributions," *Available SSRN 2529691*, 2014.

[69] J. D. Sally, *Roots to research: a vertical development of mathematical problems*. American Mathematical Soc., 2007.

[70] G. Li and R. W. Miller, *Volumetric Image Registration of Multi-modality Images of CT, MRI and PET*. INTECH Open Access Publisher, 2010.

[71] S. C. Strother, M. E. Casey, and E. J. Hoffman, "Measuring PET scanner sensitivity: relating countrates to image signal-to-noise ratios using noise equivalents counts," *Nucl. Sci. IEEE Trans. On*, vol. 37, no. 2, pp. 783–788, 1990.

[72] K. Intawong, M. Scuturici, and S. Miguet, "A New Pixel-Based Quality Measure for Segmentation Algorithms Integrating Precision, Recall and Specificity," in *Computer Analysis of Images and Patterns*, 2013, pp. 188–195.

[73] D. M. Powers, "Evaluation: from precision, recall and F-measure to ROC, informedness, markedness and correlation," 2011.

[74] F. J. Estrada and A. D. Jepson, "Benchmarking image segmentation algorithms," *Int. J. Comput. Vis.*, vol. 85, no. 2, pp. 167–181, 2009.

[75] Scion Corporation, *Scion Image ScnImage*. 2015.

[76] A. Rosset, L. Spadola, and O. Ratib, “OsiriX: an open-source software for navigating in multidimensional DICOM images,” *J. Digit. Imaging*, vol. 17, no. 3, pp. 205–216, 2004.

[77] N. S. N. Karakatsanis, N. D. N.X. Tsantilas, D. L. C. Tsoumpas, and C. R. S. G. Loudos, “Comparative evaluation of two commercial PET scanners, ECAT EXACT HR+ and Biograph 2, using GATE,” 2015.

[78] N. Karakatsanis, N. Sakellios, N. X. Tsantilas, N. Dikaios, C. Tsoumpas, D. Lazaro, G. Loudos, C. R. Schmidtlein, K. Louizi, and J. Valais, “Comparative evaluation of two commercial PET scanners, ECAT EXACT HR+ and Biograph 2, using GATE,” *Nucl. Instrum. Methods Phys. Res. Sect. Accel. Spectrometers Detect. Assoc. Equip.*, vol. 569, no. 2, pp. 368–372, 2006.

التنبؤ بجرعة المادة المشعة المناسبة للحقن في التصوير المقطعي النيتروني

ابتسام أحمد سعيد الصانع

المستخلص

لتقنيات الحاسوب والتصوير المتقدمة استخدامات واسعة النطاق في المجال الطبي و من أبرزها تقنيات التصوير الطبي مثل "التصوير المقطعي بالإشعاع النيتروني"(PET). يعتبر PET عنصر عالي الأهمية في الفحص و المعالجة السريرية لتشخيص الأمراض و تخطيط علاجها و كذلك في بحوث الأورام و اكتشافها و رصدها حيث يتيح التصوير المقطعي جمع تفاصيل عن العمليات الفسيولوجية في جسم المريض ومن ثم تحديد ما إذا كانت مرض أو عملية فسيولوجية طبيعية.

من أهم فوائد التصوير المقطعي PET في الفحص السريري هو رصد و كشف الأورام عن طريق إعطاء المريض جرعة محددة مسبقا من المادة الإشعاعية مما يسمح على سبيل المثال برؤية مفصلة و دقيقة لما يجري داخل خلايا جسم المريض. و بالتالي فإن جودة الصورة الناتجة عن عملية التصوير المقطعي تعتمد على كمية المادة الإشعاعية بالإضافة إلى الخصائص الفيزيائية لجسم المريض كالوزن والعمر و الطول فكلما زادت كمية المادة الإشعاعية زادت جودة الصورة و تزيد كفاءة الكشف عن الأورام تبعا لذلك.

يؤكد المتخصصون في التصوير المقطعي أن كل جرعة من المادة الإشعاعية ترتبط بمخاطر الإشعاع التي غالبا ما تكون مضرة للمريض . لكن الامتناع عن إجراء التصوير المقطعي بسب الخوف على المريض من مخاطر الإشعاع قد يكون اشد ضررا عليه. لهذا يجب تحديد اقل قدر ممكن من المادة الإشعاعية لتعطى للمريض و التي توفر صورة ذات جودة تشخيصيه كافية

في هذه الدراسة قمنا باقتراح أداة لمحاكاة التصوير المقطعيPET من شأنها التنبؤ بأقل جرعة ممكنة من المادة الإشعاعية لتوفير صورة تشخيصية مناسبة بناء على الخصائص الفيزيائية للمريض (الوزن و العمر)و ذلك من اجل تحسين عملية التشخيص السريري و الكشف عن الأورام

قمنا ببناء نموذج لجهاز التصوير المقطعي و بناء نموذج للمريض مكون من صورة بالرنين المغناطيسي و مقطع من مجسم رقمي للدماغ . و من ثم تمت محاكاة العمليات الفيزيائية للتصوير المقطعي باستخدام محاكاة مونت كارلو. في مرحلة التحقق قمنا بتحليل الأداء لمجموعة من المتغيرات كالتحليل المكاني و الحساسية و نسبة الانتشار. و لتقييم الأداة قمنا بتنفيذ ١١ تجربة محاكاة للتنبؤ عن الجرعة لمجموعة مكونة من ٦٠ مريض.

و لقد وجدنا أن أداة التنبؤ استطاعت و بكفاءة التنبؤ بجرعات المادة المشعة المناسبة للحقن و بنسبة تحسين تصل إلى ٢٨% بالنسبة للجرعات المعتمدة في الفحص السريري حاليا. كما وجدنا أن جرعات المادة المشعة للمرضى البالغين تتأثر في الغالب بوزن المريض بدلا من عمر المريض.